EG&G Idaho, Inc.

FORM EG&G-398
(Rev. 11-79)

INTERIM REPORT

Accession No. _____

Report No. EGG-CDAP-5439

Contract Program or Project Title:
Fuel Behavior Model Development Program

Subject of this Document: Developmental Assessment of FRAP-T6

Type of Document: Internal Report

Author(s): L. J. Siefken

NRC Research and Technical Assistance Report

Date of Document: May 1981

Responsible NRC Individual and NRC Office or Division: G. P. Marino - NRC-RSR

This document was prepared primarily for preliminary or internal use. It has not received full review and approval. Since there may be substantive changes, this document should not be considered final.

EG&G Idaho, Inc.
Idaho Falls, Idaho 83415

Prepared for the
U.S. Nuclear Regulatory Commission
Washington, D.C.
Under DOE Contract No. DE-AC07-76ID01570
NRC FIN No. A6050

INTERIM REPORT

DEVELOPMENTAL ASSESSMENT OF FRAP-T6

EGG-CDAP-5439
MAY 1981

L. J. Siefken

Prepared For:
U. S. Nuclear Regulatory Commission
Under DOE Contract Number DE-AC07-76ID01570
Fin. No. A6050

ABSTRACT

The FRAP-T6 computer code is assessed for applicability and accuracy by comparing calculations of the code with the data of well characterized steady state and transient fuel rod tests. The comparisons show that the code is capable of analyzing fuel rod performance during operational transients and hypothetical reactor accidents. The code overpredicts fuel rod temperatures by 0 to 5% prior to the time of DNB and by 0 to 20% after the time of DNB. The code accurately calculates the extent of cladding ballooning and the time of cladding rupture. The FRAP-T6 computer code is capable of calculating transient fission gas release over a wide range of fuel temperatures. The code is improved over its predecessor, FRAP-T5, both in modeling capabilities and in operational efficiency.

ACKNOWLEDGEMENTS

The author gratefully acknowledges C. S. Watson for performing the computer analyses and plotting the calculation results, and Kathy Wesley for typing the report.

CONTENTS

FIGURES

TABLES

DEVELOPMENTAL ASSESSMENT OF FRAP-T6

1. INTRODUCTION

The ability to accurately predict the performance of light water reactors (LWRs) during various operational transients and hypothetical accidents is a major objective of the Reactor Safety Research Program being conducted by the U. S. Nuclear Regulatory Commission (NRC). The NRC is sponsoring experiments such as those performed in the LOFT and PBF facilities[1] to learn firsthand the performance of a LWR and its fuel rods during operational transients and hypothetical accidents. In addition, the NRC is sponsoring the development of computer codes to predict the performance of different LWR designs for a broad range of transients. The computer codes are assessed for applicability and accuracy with benchmark data provided by the experiments. The computer codes under development include reactor system analysis codes to calculate transient reactor power and coolant conditions and fuel rod analysis codes to calculate fuel rod performance.

The computer code developed for the calculation of the performance of LWR fuel rods during operational transients and hypothetical accidents is the Fuel Rod Analysis Program--Transient (FRAP-T6) code,[2] which is the sixth and final in a series of code versions. The FRAP-T6 code has the capability of modeling all of the phenomena which influence the performance of a fuel rod. The code has a heat conduction model to calculate the stored energy in the fuel and the transfer of heat from the fuel to the cladding. The code has a cooling model to calculate the transfer of heat from the cladding to the coolant. Mechanical response models are included to calculate the deformation of the fuel and cladding. A fission gas release model is included to calculate the migration of the noble fission gases from the fuel to the fuel-cladding gap.

The assessment of the FRAP-T6 code is divided into a developmental assessment task and an independent assessment task. In the developmental assessment task, the code calculations are compared in-depth with the experimental data from a few well-characterized fuel rod tests. A phenomenological analysis of the code calculations is performed. In the

independent assessment task, the code calculations are compared with the experimental data of a large number of fuel rod tests. A statistical analysis of the calculations is performed. This report describes the development assessment of the FRAP-T6 code.

The developmental assessment of FRAP-T6 achieves four objectives:

1. The code is checked for applicability and accuracy by comparing the code calculations with reliable experimental data.
2. The reasons for discrepancies between the code calculations and the experimental data are determined.
3. The code calculations are compared with the calculations of its predecessor, FRAP-T5,[3] to quantify improvements.
4. The code is exercised over a broad range of fuel rod transients to test the analysis capability for all types of hypothetical accidents.

The developmental assessment of FRAP-T6 focuses on the assessment of the temperature, cladding ballooning and fission gas release models. The temperature model is assessed by comparing calculated fuel centerline temperatures with the temperatures measured during steady state and transient tests. In addition, the calculated fuel stored energy is assessed by comparing calculated and measured temperatures at locations between the fuel centerline and fuel surface. The critical heat flux and heat transfer correlations are assessed by comparing calculated and measured cladding surface temperature for fuel rod tests in which film boiling occurred. The cladding ballooning models are assessed by comparing calculated and measured internal gas pressure for tests in which cladding ballooning occurred. The cladding ballooning models are also assessed by a comparison of calculated and measured post-test cladding diameters. The fission gas release model is assessed by comparing calculated and measured fission gas release. Correct modeling of circumferentially varying coolant conditions is demonstrated by showing the results of an example analysis.

The developmental assessment report is divided into eight sections. The temperature model is assessed in Section 2. The critical heat flux and heat transfer correlations are assessed in Section 3. The assessment of the cladding ballooning models is described in Section 4. The assessment of the fission gas release model is described in Section 5. Correct modeling of circumferentially varying coolant conditions is demonstrated in Section 6. The assessment of several additional modeling features is discussed in Section 7. Section 8 presents the conclusions of the FRAP-T6 developmental assessment. A list of the differences between FRAP-T5 and FRAP-T6 is given in Appendix A. A list of the fuel rod tests and hypothetical accidents analyzed with FRAP-T6 is given in Appendix B.

2. ASSESSMENT OF TEMPERATURE MODEL

The temperature model is the most important model in FRAP-T6. The temperature model applies the laws of thermodynamics and heat conduction to calculate the temperature throughout a fuel rod. Most of the other models are strongly influenced by the calculated temperatures. Therefore, the temperature model must first be examined to verify that it is not distorting the calculations of the other models.

A comparison of fuel deformation models is included in the assessment of the temperature model. The fuel deformation models calculate the size of the fuel-cladding gap and the size of circumferential cracks in the fuel. The temperature model is influenced by the values of these variables. Three fuel deformation models are available in FRAP-T6. The code user selects which one of the three models is to be used. The three models are: (a) the FRACAS-I model with a nonuniform fuel-cladding gap (b) the FRACAS-I model with fuel relocation and circumferential cracking of the fuel, and (c) the FRACAS-II model with fuel relocation and circumferential cracking of the fuel. The temperature model is assessed using both the FRACAS-I model with a nonuniform fuel-cladding gap and the FRACAS-I model with fuel relocation. The calculated temperatures are compared with measured temperatures to determine which of the two mechanical response models results in the best calculation of temperature. Since the temperatures calculated using either the FRACAS-I model

with relocation or the FRACAS-II model are almost identical, the latter mechanical response model is not considered.

The first part of the assessment of the temperature model consists of comparisons of calculated and measured temperatures when steady state conditions exist. Given constant fuel rod power and cooling, a transient temperature model should calculate the measured temperature distribution. Close agreement between calculated and measured temperatures indicates that the transient temperature model is correctly modeling heat transfer across the fuel-cladding gap and heat conduction in the fuel.

The second part of the assessment of the temperature model consists of comparisons of calculated and measured temperatures when transient conditions exist. In addition to assessing the modeling of heat transfer across the fuel-cladding gap and heat conduction in the fuel, these transient temperature comparisons also assess the modeling of the heat capacity of the fuel and cladding.

2.1 Steady State Fuel Temperature Comparisons

The steady state fuel temperature assessment is divided into four sections. In Section 2.1.1, the calculated and measured fuel centerline temperatures for 15 by 15 PWR fuel rods are compared. In Section 2.1.2, the calculated and measured fuel centerline temperatures for 8 by 8 BWR fuel rods are compared. In Section 2.1.3, the calculated and measured fuel centerline temperatures for fuel rods containing xenon and argon fill gas are compared. In Section 2.1.4, the calculated and measured fuel off-center temperatures are compared.

2.1.1 PWR Fuel Rod Comparisons (15 by 15). The experimental data of three tests are used to assess the temperature calculations for 15 by 15 PWR fuel rods. The three tests are: (a) the LOC-1C test[4] performed in the Power Burst Facility (PBF), (b) the IFA-508 test[5] performed in the Halden Boiling Water Reactor (HBWR), and (c) the IFA-430 test[6] performed in HBWR. The design characteristics of the test fuel rods are shown in Tables 1, 2 and 3, respectively.

The calculated and measured fuel centerline temperatures for the three tests are compared in Figures 1, 2 and 3, respectively. The

TABLE 1. CHARACTERISTICS OF ROD 3 OF PBF TEST LOC-11C

Characteristic	Value
Fuel Enrichment (Wt % U^{235})	10.0
Fuel Density (% Theoretical Density)	94.4
Radial Fuel-cladding gap (mm)	0.105
Cladding Thickness (mm)	0.606
Cladding Outside Diameter(mm)	10.72
Fuel Pellet Outside Diameter (mm)	9.29
Fill Gas composition	Helium
Fill Gas Pressure (MPa)	2.22
Burnup (MWs/kg)	0
Active Fuel Stack Length (m)	0.915
Plenum Volume (mm^3)	3720
Axial Power Peaking Factor	1.40
Cladding Cold Work (%)	20
Diameter of Hole for Thermocouple at Center of Fuel (mm)	1.88

TABLE 2. CHARACTERISTICS OF ROD 13 OF HBWR TEST IFA-508

Characteristic	Value
Fuel Enrichment (wt % U^{235})	10.5
Fuel Density (% Theoretical Density)	95
Radial Fuel-cladding gap (mm)	0.11
Cladding Thickness (mm)	0.34
Cladding Outside Diameter (mm)	12.20
Fuel Pellet Outside Diameter (mm)	11.30
Fill Gas Composition	Helium
Fill Gas Pressure (MPa)	0.103
Burnup (MWs/kg)	0
Active Fuel Stack Length (m)	0.39
Plenum Volume (mm^3)	6240
Axial Power Peaking Factor	1.1
Cladding Cold Work (%)	10
Diameter of Hole for Thermocouple at Center of Fuel (mm)	1.80

TABLE 3. CHARACTERISTICS OF ROD 2 OF IFA-430 TEST

Characteristic	Value
Fuel Enrichment (wt % U^{235})	10.0
Fuel Density (% Theoretical Density)	94.6
Radial Fuel-cladding gap (mm)	0.115
Cladding Thickness (mm)	0.94
Cladding Outisde Diameter (mm)	12.79
Fuel Pellet Outside Diameter (mm)	10.68
Fill Gas Composition	100% He or 90% He, 10% Xe
Fill Gas Pressure (MPa)	5.1
Burnup (MWs/kg)	0
Active Fuel Stack Length (m)	1.28
Plenum Volume (m^3)	10
Axial Power Peaking Factor	1.26
Cladding Cold Work (%)	10
Diameter of Hole for Thermocouple at Center of Fuel (mm)	1.88

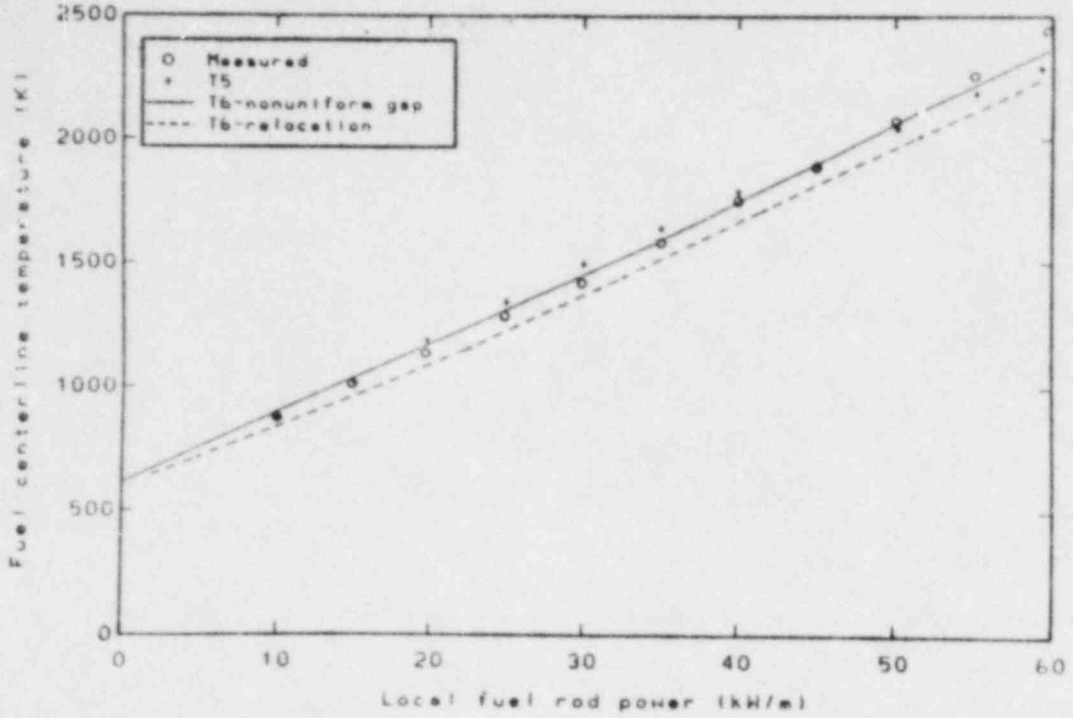

Figure 1. Comparison of measured and calculated fuel centerline temperature versus local rod power for Rod 3 of PBF test LOC-11C.

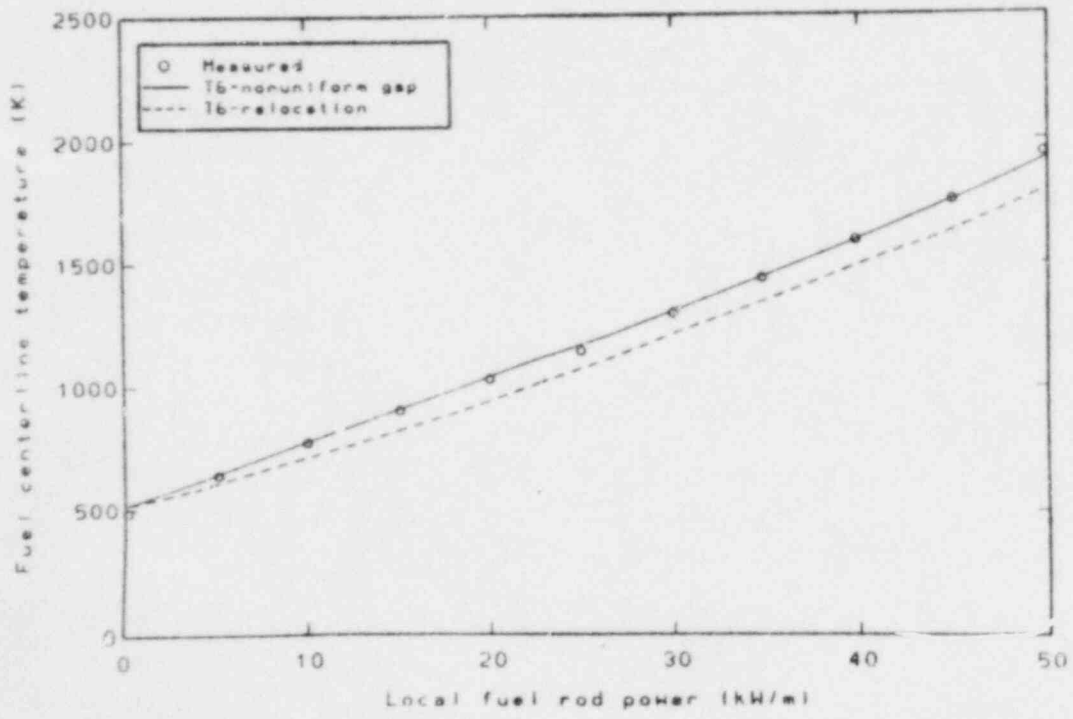

Figure 2. Comparison of measured and calculated fuel centerline temperature versus local rod power for Rod 13 of HBWR test IFA-508.

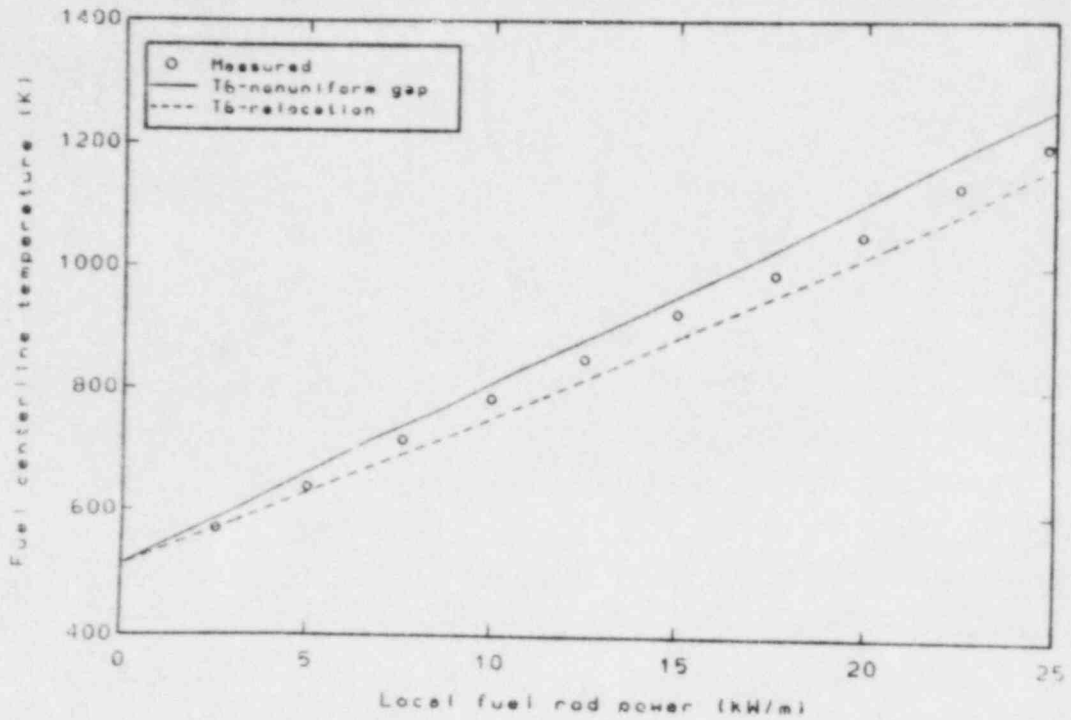

Figure 3. Comparison of measured and calculated fuel centerline temperature versus local rod power for Rod 2 of HBWR test IFA-430 with 100% helium.

temperatures are calculated using boch the FRACAS-I model with a nonuniform fuel-cladding gap model and the FRACAS-I model with fuel relocation. For the LOC-11C and IFA-508 tests, the nonuniform gap model calculates fuel centerline temperatures that are greater than the measured values by 0 to 1% in the 0 to 50 kW/m range of power. The relocation model calculates fuel centerline temperatures that are less than measured values by 3 to 5% in the 0 to 50 kW/m range of power. For the IFA-430 test, the nonuniform gap model calculates fuel centerline temperatures that are 3 to 5% greater than the measured temperatures, and the relocation model calculates fuel centerline temperatures that are 3 to 5% less than the measured temperatures. For a fuel rod power greater than 55 kW/m, the centerline temperature comparisons of Figure 1 show that both models calculate fuel temperatures which are less than the measured values. At a fuel rod power of 60 kW/m, the nonuniform gap model calculates a fuel centerline temperature which is less than measured value by 4%, and the relocation model calculates fuel centerline temperature which is less than measured value by 8%.

In Figure 1, the calculations of FRAP-T6 are also compared with those of FRAP-T5. The calculations of FRAP-T6 with the nonuniform gap model are in closer agreement with the measurements than the FRAP-T5 calculations. At a fuel rod power of 30 kW/m, FRAP-T6 calculates a centerline temperature which is greater than measured value by 40 K, while FRAP-T5 calculates temperatures which are less than the measured values by 80 K. At a fuel rod power of 60 kW/m, FRAP-T6 calculates a centerline temperature 80 K less than the measured temperature, while FRAP-T5 calculates a centerline temperature 150 K less than the measured temperature.

2.1.2 BWR Fuel Rod Comparisons (8 by 8). The experimental data of Rod 1 of PBF Test PR-1[7] are used to assess temperature calculations for 8 by 8 BWR fuel rods. The design characteristics of the test fuel rod are shown in Table 4.

The calculated and measured fuel centerline temperatures are

TABLE 4. CHARACTERISTICS OF RODS 1 AND 4 OF PBF TEST PR-1

Characteristic	Value
Fuel Enrichment (wt % U^{235})	10
Fuel Density (% Theoretical Density)	95 (Rod 1) 97 (Rod 4)
Radial Fuel-cladding gap (mm)	0.11
Cladding Thickness (mm)	0.855
Cladding Outside Diameter (mm)	12.50
Fuel Pellet Outside Diameter (mm)	10.57
Fill Gas Composition	He (Rod 1) Ar (Rod 4)
Fill Gas Pressure (MPa)	2.59
Burnup (MWs/kg)	0
Active Fuel Stack Length (m)	0.913
Plenum Volume (mm^3)	27400
Axial Power Peaking Factor	1.33
Cladding Cold Work (%)	10%
Diameter of Hole for Thermocouple at Center of Fuel (mm)	1.78

compared in Figure 4. The temperatures are calculated using both the FRACAS-I model with a nonuniform fuel-cladding gap model and the FRACAS-I model with fuel relocation. The temperatures calculated using the nonuniform gap model are 2% less than the measured temperatures. The temperatures calculated using the fuel relocation model are 6 to 9% less than the measured temperatures.

2.1.3 Xenon and Argon Filled Fuel Rod Comparisons. A more complete assessment of the models for fuel-cladding gap heat transfer and fuel relocation is available from the results of tests performed on xenon and argon filled fuel rods. The more complete assessment is possible because the temperature drop across the fuel-cladding gap of xenon and argon filled fuel rods is much larger than that for helium filled fuel rods. At a fuel rod power of 30 kW/m, for example, the temperature drop across the fuel-cladding gap is about 200 K for a helium filled rod and 750 K for a xenon filled rod. As a result, the temperature drop across the fuel-cladding gap is reflected more in the fuel centerline temperature measurements of xenon and argon filled fuel rods than of helium filled fuel rods.

The experimental data of three test fuel rods are used to assess fuel centerline temperature calculations for fuel rods filled with xenon and argon. The three rods are Rod 2 of the IFA-430 test[6] performed in the HBWR, Rod 4 of the PR-1 test[7] performed in PBF, and Rod 501 of the GC 2-1 test[8] performed in PBF. For the IFA-430 test, the fuel rod fill gas was a mixture of 90% helium and 10% xenon. The other characteristics of the fuel rod are shown in Table 4. For the GC 2-1 test, the fill gas was xenon. The other characteristics of the fuel rod are shown in Table 5.

The calculated and measured fuel centerline temperatures are compared in Figures 5, 6 and 7. The temperatures are calculated using both the FRACAS-I model with a nonuniform fuel-cladding gap model and the FRACAS-I model with fuel relocation. For the IFA-430 test (90% He, 10% Xe), the fuel centerline temperatures calculated using the nonuniform gap model are 6 to 7% greater than the measured temperatures. For Rod 4 of the PR-1 test, the fuel centerline temperatures calculated using the nonuniform gap model are greater than the measured fuel centerline temperatures by 4% at 20 kW/m and by 5% at 40 kW/m. For the same test,

TABLE 5. CHARACTERISTICS OF RODS 501 AND 503 OF PBF TEST GC 2-1

Characteristic	Value
Fuel Enrichment (wt % U^{235})	10.0
Fuel Density (% Theoretical Density)	97 (Rod 501) 95 (Rod 503)
Radial Fuel-Cladding Gap (mm)	0.11
Cladding Thickness (mm)	0.855
Cladding Outside Diameter (mm)	12.50
Fuel Pellet Outside Diameter (mm)	10.57
Fill Gas Composition	Xe (Rod 501) He (Rod 503)
Fill Gas Pressure (MPa)	2.59
Burnup (MWs/kg)	0
Active Fuel Stack Length (m)	0.913
Plenum Volume (mm^3)	27400
Axial Power Peaking Factor	1.33
Cladding Cold Work (%)	10
Diameter of Hole for Themocouple at Center of Fuel (mm)	1.78

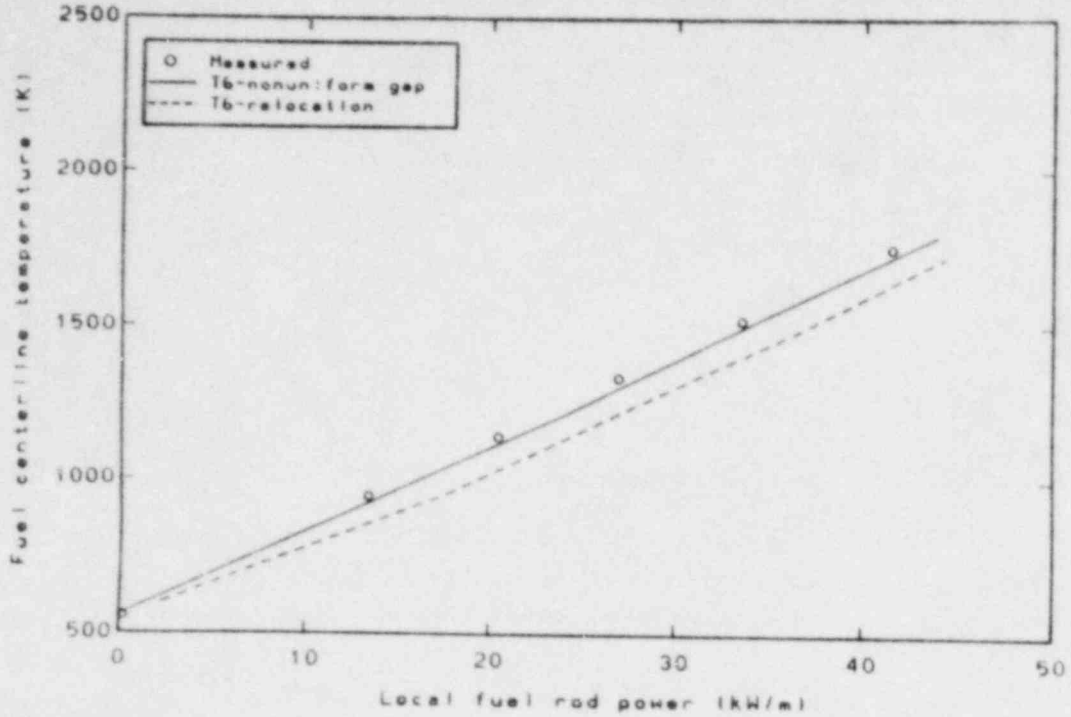

Figure 4. Comparison of measured and calculated fuel centerline temperature versus local rod power for Rod 1 of PBF test PR-1.

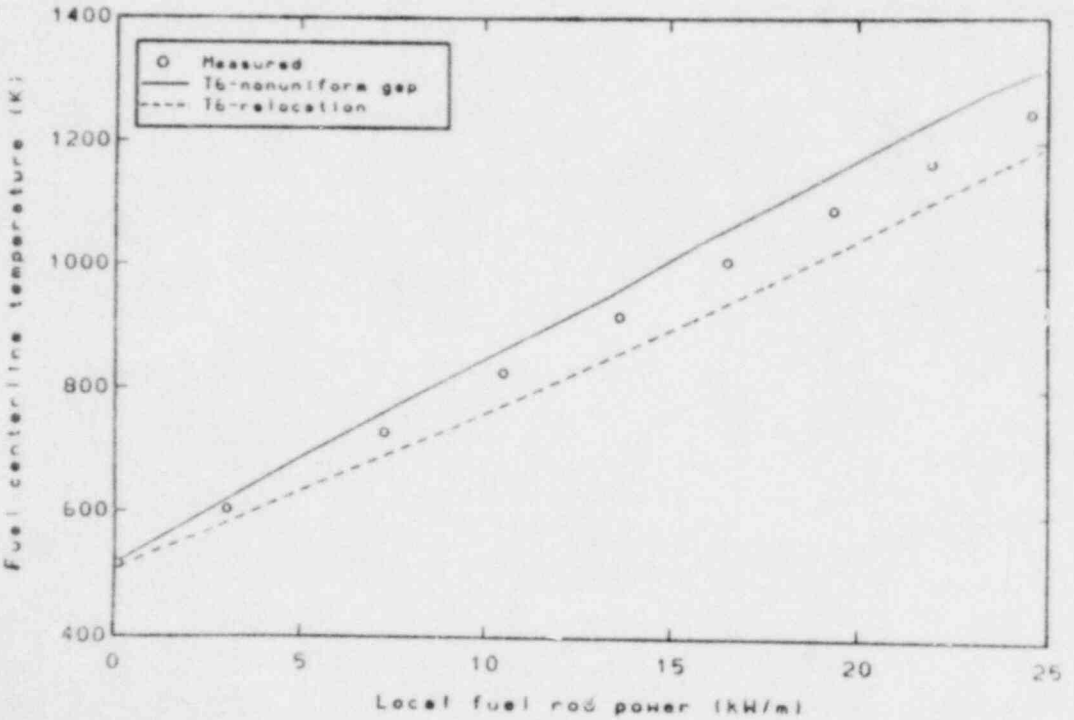

Figure 5. Comparison of measured and calculated fuel centerline temperature versus local rod power for Rod 2 of HBWR test IFA-430 with 90% helium and 10% xenon.

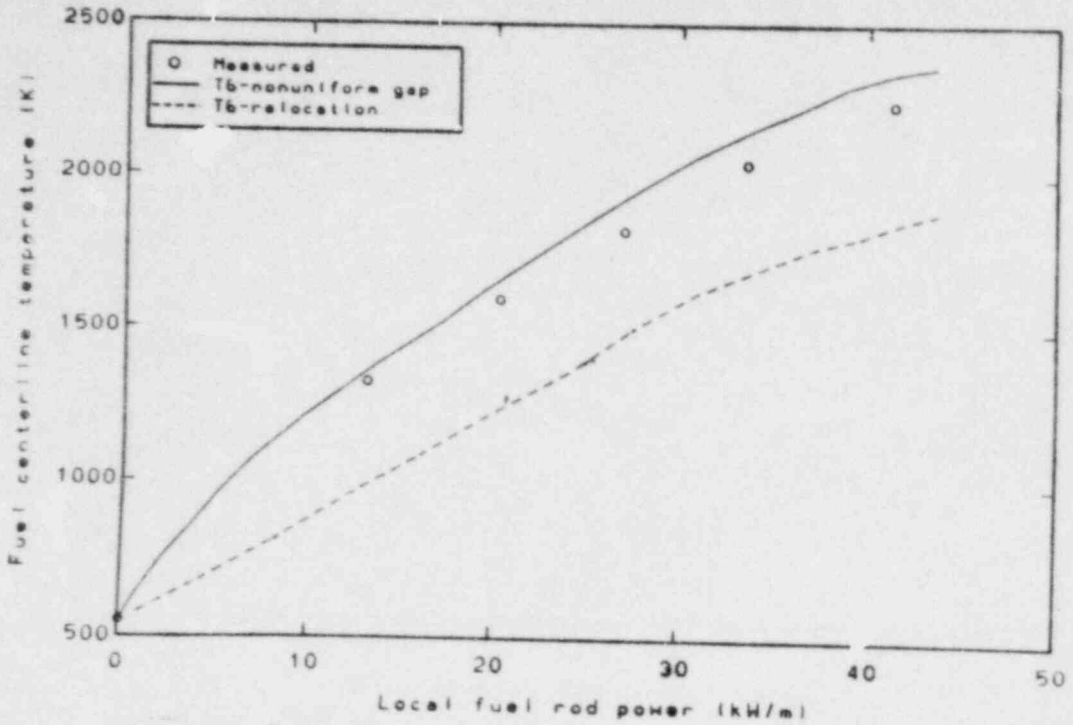

Figure 6. Comparison of measured and calculated fuel centerline temperature versus local rod power for Rod 4 of PBF test PR-1.

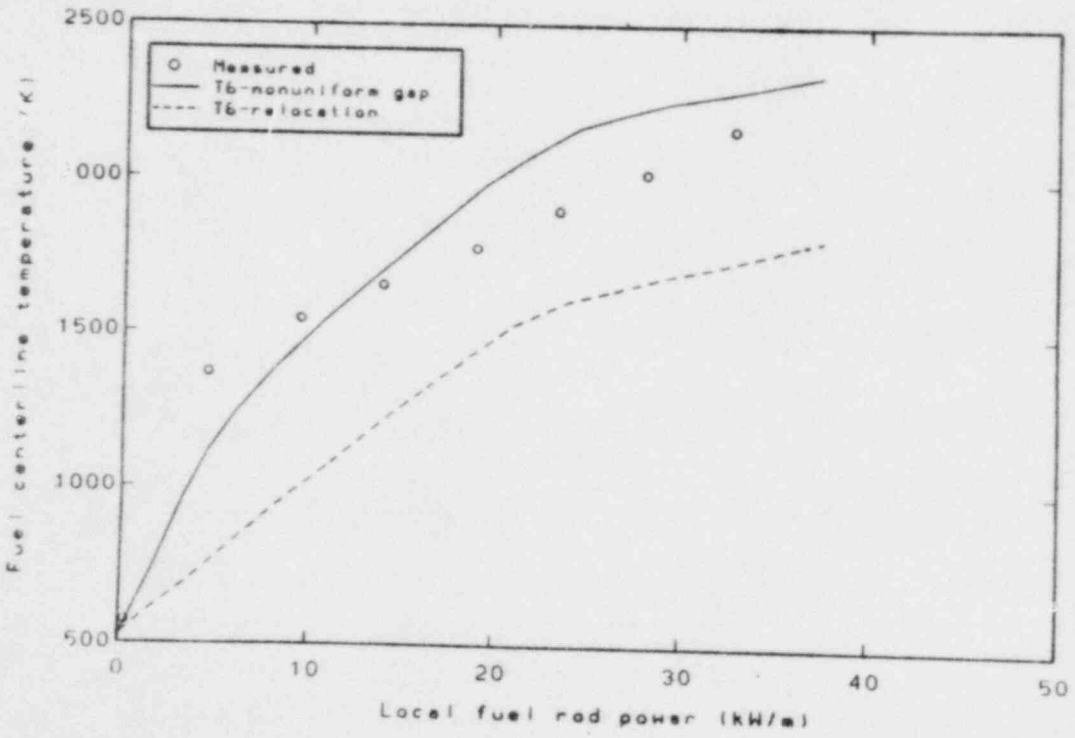

Figure 7. Comparison of measured and calculated fuel centerline temperature versus local rod power for Rod 501 of PBF test GC 2-1.

the fuel centerline temperatures calculated using the relocation model are less than the measured temperatures by 22% at 10 kW/m and by 18% at 40 kW/m. For rod 501 of the GC 2-1 test, the temperatures calculated using the nonuniform gap model are less than the measured fuel centerline temperatures for fuel rod powers less than 12 kW/m. The calculated temperatures are 5% less than the measured values at 10 kW/m and 10% greater than the measured values at 20 to 30 kW/m. For the same test, the fuel centerline temperatures calculated using the relocation model are less than the measured values over the compete range of power. The calculated temperature is 33% less than the measured value at 10 kW/m and 18% less than the measured value at 26 kW/m. Since thermocouple shunting is speculated to have occurred during this test,[8] the actual fuel centerline temperature was probably greater than the measured temperature for a fuel rod power greater than 25 kW/m.

2.1.4 Stored Energy. The amount of thermal energy stored in the fuel at the start of a reactor transient can play an important role in the response of the fuel rod during the transient. The amount of stored energy is not only a function of the temperature at the fuel center, but is also a function of the temperature gradient from the fuel center to the fuel surface. A steep temperature gradient can result in 15% less stored energy than a shallow gradient. In order to measure the fuel temperature gradient, a series of tests were performed in PBF with thermocouples placed at points between the fuel center and the fuel surface. This series of tests included PBF tests GC 2-1,[8] GC 2-2,[8] and PR-1.[7] The experimental data from these tests are used to assess the temperature gradient and stored energy calculated by the FRAP-T6 code.

Four thermocouples were placed in the fuel of the test rods for PBF tests GC 2-1, GC 2-2, and PR-1. The thermocouples were positioned as shown in Figure 8. One thermocouple was placed at the center of the fuel, and three thermocouples were offset from the center. The distance from the fuel center to the center of each of the offset thermocouples was equal to 75% of the fuel pellet radius. The offset

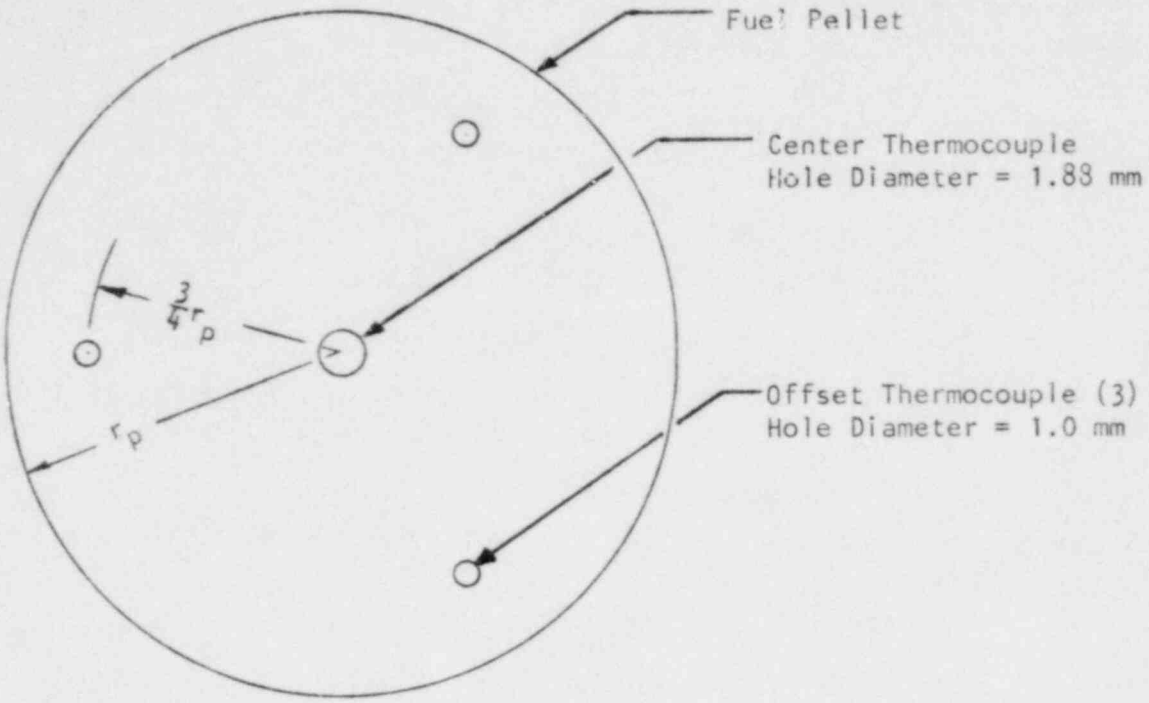

Figure 8. Positions of the centerline and offset thermocouples for PBF tests GC 2-1, GC 2-2 and PR-1.

thermocouples were azimuthally spaced 120 degrees apart.

Except for fuel density and fill gas, the test fuel rods were typical of 8 by 8 BWR fuel rods. The design characteristics of the test fuel rods are shown in Tables 4, 5 and 6.

The fuel temperature distribution is calculated using both the FRACAS-I model with a nonuniform fuel-cladding gap and the FRACAS-I model with fuel relocation. For the nonuniform gap model, the temperature is calculated using both the one-dimensional (radial) and the two-dimensional (radial-azimuthal) heat conduction models. The relocation model assumes fuel relocation to be azimuthally uniform. Therefore, the temperature distribution using this fuel deformation model is axisymmetric and the two-dimensional heat conduction calculation is not necessary.

The calculated and measured fuel temperatures for a small gap (0.05 mm) helium filled rod (Rod 521-3 of PBF test GC 2-2) are compared in Table 7. Those for a typical gap (0.11 mm) helium filled rod (Rod 503 of PBF test GC 2-1 and Rod 1 of PBF test pr-1) are compared in Tables 8 and 9, respectively. The fuel temperatures calculated with the one-dimensional nonuniform gap model are in good agreement with the measured fuel temperatures. For all three tests, the fuel temperature calculated at the radius of the offset thermocouples is within the range of fuel temperatures measured by the offset thermocouples. The temperatures calculated with the relocation model are 10 to 15% less than the measured values. The temperatures are underpredicted at both the fuel center and the radius of the offset thermocouple. The calculated temperature gradient, however, is in good agreement with the measured temperature gradient.

Except for Rod 1 of the PR-1 test, the temperatures calculated with the two-dimensional heat conduction model at the locations of the offset thermocouples are in good agreement with the temperatures measured by the offset thermocouples. For Rod 1 of the PR-1 test, the calculated temperatures bracket the measured temperatures, but have a much greater azimuthal temperature variation than the measured temperatures. The small azimuthal temperature variation measured for Rod 1 of the PR-1 test is inconsistent with the measured azimuthal temperature variation of the other tests and is considered an anomaly.

TABLE 6. CHARACTERISTICS OF ROD 522-3 OF PBF TEST GC 2-2

Characteristic	Value
Fuel Enrichment (wt % U^{235})	10.0
Fuel Density (% Theoretical Density)	95
Radial Fuel-cladding Gap (mm)	0.05
Cladding Thickness (mm)	0.855
Cladding Outside Diameter (mm)	12.5
Fuel Pellet Outside Diameter (mm)	10.69
Fill Gas Composition	Helium
Fill Gas Pressure (MPa)	2.59
Burnup (MWs/kg)	0
Active Fuel Stack Length (m)	3.913
Plenum Volume (mm^3)	27400
Axial Power Peaking Factor	1.33
Cladding Cold Work (%)	10
Diameter of Hole for Thermocouple at Center of Fuel	1.78

TABLE 7. COMPARISON OF MEASURED AND CALCULATED TEMPERATURE DISTRIBUTION FOR ROD 522-3 OF PBF TEST GC 2-2

Local Power = 31.4 kW/m

Position[a]	Measured Temperature (K)	2-D Calculated Temperature (K)	Nonuniform gap Calculated Temperature (K)	Relocation Calculated Temperature (K)
Centerline	1360	1223	1267	1208
Offset 1	1010	995	970	908
Offset 2	955	--	--	--
Offset 3	X[b]	963	--	--

a. The offset thermocouple with the highest temperature reading was arbitrarily assigned position 1, the thermocouple with the lowest reading was assigned position 3.

b. The symbol "X" indicates that no measurement was obtained due to thermocouple failure.

TABLE 8. COMPARISON OF MEASURED AND CALCULATED TEMPERATURE DISTRIBUTION FOR ROD 503 OF PBF TEST GC 2-1

Local Power = 20.6 kW/m

Position[a]	Measured Temperature (K)	2-D Calculated Temperature (K)	Nonuniform gap Calculated Temperature (K)	Relocation Calculated Temperature (K)
Centerline	1200	1111	1134	1042
Offset 1	970	1066	944	816
Offset 2	900	973	--	--
Offset 3	840	850	--	--

a. The offset thermocouple with the highest temperature reading was arbitrarily assigned position 1, and the thermocouple with the lowest reading was assigned position 3.

TABLE 9. COMPARISON OF MEASURED AND CALCULATED TEMPERATURE DISTRIBUTION FOR ROD 1 OF PBF TEST PR-1

Local Power = 27 kW/m

Position[a]	Measured Temperature (K)	2-D Calculated Temperature (K)	Nonuniform gap Caculated Temperature (K)	Relocation Calculated Temperature (K)
Centerline	1320	1291	1313	1215
Offset 1	1045	1294	1043	900
Offset 2	1020	--	--	--
Offset 3	1010	941	--	--

a. The offset thermocouple with the highest temperature reading was arbitrarily assigned position 1, the thermocouple with the lowest reading was assigned position 3.

The calculated and measured fuel temperatures for a xenon filled fuel rod (Rod 501 of PBF test GC 2-1) at a local power of 20.6 kW/m are compared in Table 10. The temperatures measured by the offset thermocouples ranged from 1480 to 1670 K (average of 1575 K). The temperatures calculated with the one-dimensional nonuniform gap model are 160 K greater than both the measured fuel centerline temperatures and the average measured offset temperatures. The fuel temperatures calculated with the relocation model are 340 K less than the measured values at both the fuel centerline and the locations of the offset thermocouples. The same temperature gradient is calculated with both the nonuniform gap model and the relocation model, but a 500 K higher temperature drop across the fuel-cladding gap is calculated with the nonuniform gap model. The temperatures calculated with the two-dimensional nonuniform gap model are 200 K greater than the temperatures measured by the offset thermocouples. The calculated azimuthal temperature variation, however, is in good agreement with the measured azimuthal temperature variation.

2.2 Transient Temperature Comparisons

The assessment of the transient temperature calculations is divided into two sections. In Section 2.2.1, the assessment focuses on the modeling of the heat capacity of the fuel and cladding. In Section 2.2.2, the assessment focuses on the modeling of heat removal from the fuel.

2.2.1. Assessment of the Modeling of Heat Capacity. The modeling of the fuel and cladding heat capacity is assessed by comparison of the calculated and measured temperatures for fuel rod tests performed under nearly adiabatic heatup conditions. Two fuel rod tests are selected for comparisons. The first rod is Rod 12 of TREAT FRF-2 test,[9] during which the test fuel rod was subjected to a power pulse with an average amplitude of 20 kW/m and a duration of 30 s. The test fuel rod was cooled by superheated steam, which resulted in

TABLE 10. COMPARISON OF MEASURED AND CALCULATED TEMPERATURE DISTRIBUTION FOR ROD 501 OF PBF TEST GC 2-1

Local Power = 20.6 kW/m

Position[a]	Measured Temperature (K)	2-D Calculated Temperature (K)	Nonuniform gap Calculated Temperature (K)	Relocation Calculated Temperature (K)
Centerline	1850	1982	2013	1512
Offset 1	1670	1863	1729	1239
Offset 2	X[b]	--	--	--
Offset 3	1480	1654	--	--

a. The offset thermocouple with the highest temperature reading was arbitrarily assigned position 1 and the thermocouple with the lowest reading was assigned position 3.

b. The symbol "X" indicates that no measurement was obtained due to thermocouple failure.

little heat removal from the fuel rod. The design characteristics of the test fuel rod are shown in Table 11. The second rod is Rod 3 of the PBF RIA 1-1 test,[9] during which the test fuel rod was subjected to burst of power with a peak amplitude of 15,000 kW/m and a duration of 0.1 s. The test fuel rod was subjected to coolant conditions typical of those occurring during normal reactor operation. The design characteristics of the test fuel rod are shown in Table 12.

The calculated and measured cladding surface temperatures for Rod 12 of the TREAT FRF-2 test are compared in Figure 9. The comparison is for an elevation of 0.28 m above the bottom of the fuel stack. The entire fuel rod is initially at the temperature of the steam cooling the fuel rod. The fuel rod is then subjected to a power of approximately 20 kW/m for 30 s and is cooled by low flow superheated steam to simulate heat transfer during the reflood period of a loss of coolant accident (LOCA). Nearly adiabatic heatup of the fuel rod occurs because of the low coolant flow. The calculated and measured temperatures agree closely over most of the time interval of the transient. For the time interval of 25 to 35 s, the calculated cladding temperature is greater than the measured temperature. The maximum difference between the calculated and measured temperature is 50 K. The discrepancy is due to bypassing of the cladding oxidation model. The low calculation of temperature begins at about the time that some cladding heatup due to cladding oxidation occurs. The cladding oxidation is not modeled, however, because cladding oxidation is restricted by the small amount of oxygen available in the low steam flow. Oxygen limited cladding oxidation cannot be modeled by FRAP-T6. After a time of 40 s, the cladding temperature is calculated to increase showly with time, but the measured temperature remains constant with time. This difference is due to the neglecting of radiation heat transfer to the flow shroud in the calculation of temperature.

The calculated and measured fuel centerline temperatures for Rod 3 of the PBF RIA 1-1 test are compared in Figure 10. In this test, the test rod fuel at the elevation of the fuel temperature measurement was heated to an enthalpy of 165 cal/g in 0.1 s by a high intensity short

TABLE 11. CHARACTERISTICS OF ROD 12 OF TREAT TEST FRF-2

Characteristic	Value
Fuel Density (% Theoretical Density)	95
Radial Fuel-Cladding Gap (mm)	0.061
Cladding Thickness (mm)	0.813
Cladding Outside Diameter (mm)	14.31
Fuel Pellet Outside Diameter (mm)	12.56
Fill Gas Composition	He
Fill Gas Pressure (MPa)	0.517
Burnup (MWs/kg)	0
Active Fuel Stack Length (m)	0.635
Plenum Volume (mm^3)	9000
Axial Power Peaking Factor	1.1
Cladding Cold Work (%)	10

TABLE 12. CHARACTERISTICS OF ROD 3 OF PBF TEST RIA 1-1

Characteristic	Value
Fuel Enrichment (wt % U^{235})	12.5
Fuel Density (% Theoretical Density)	94.5
Radial Fuel-Cladding Gap (mm)	0.167
Cladding Thickness (mm)	0.533
Cladding Outside Diameter (mm)	9.93
Fuel Pellet Outside Diameter (mm)	8.53
Fill Gas Composition	He
Fill Gas Pressure (MPa)	0.103
Burnup (MWs/kg)	0
Active Fuel Stack Length (m)	0.914
Plenum Volume (mm^3)	4650
Axial Power Peaking Factor	1.36
Cladding Cold Work (%)	10
Diameter of Hole for Thermocouple of Fuel Center (mm)	1.8

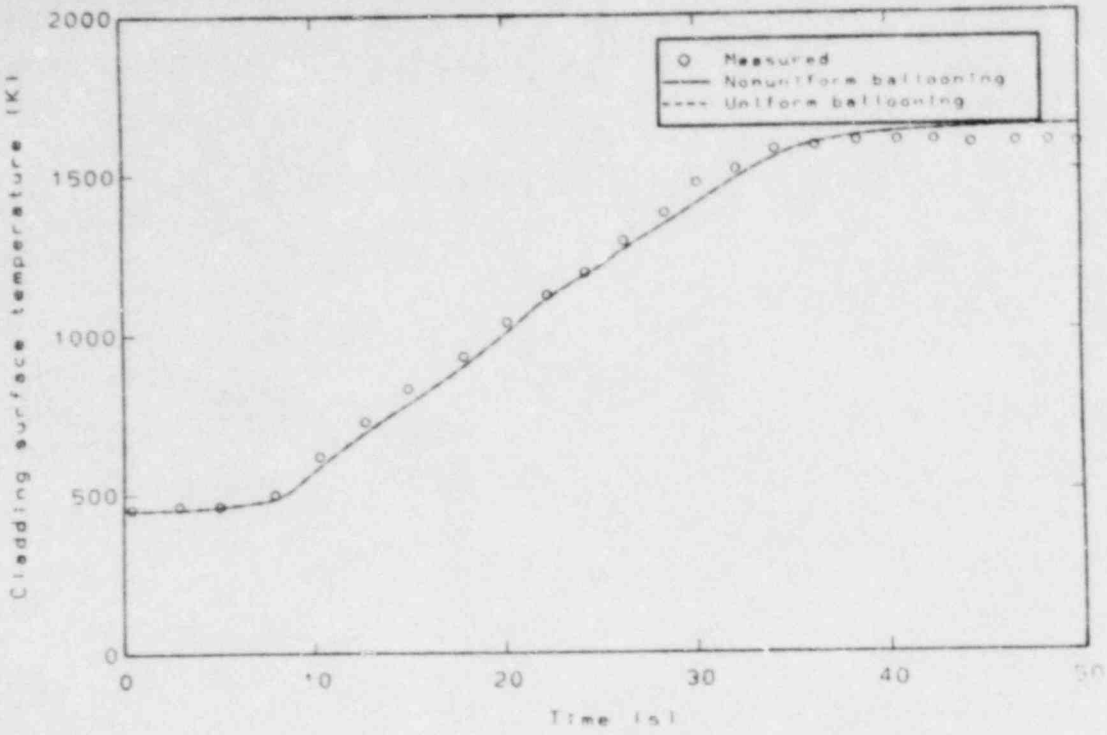

Figure 9. Comparison of measured and calculated cladding surface temperature versus time for Rod 12 of the TREAT test FRF-2.

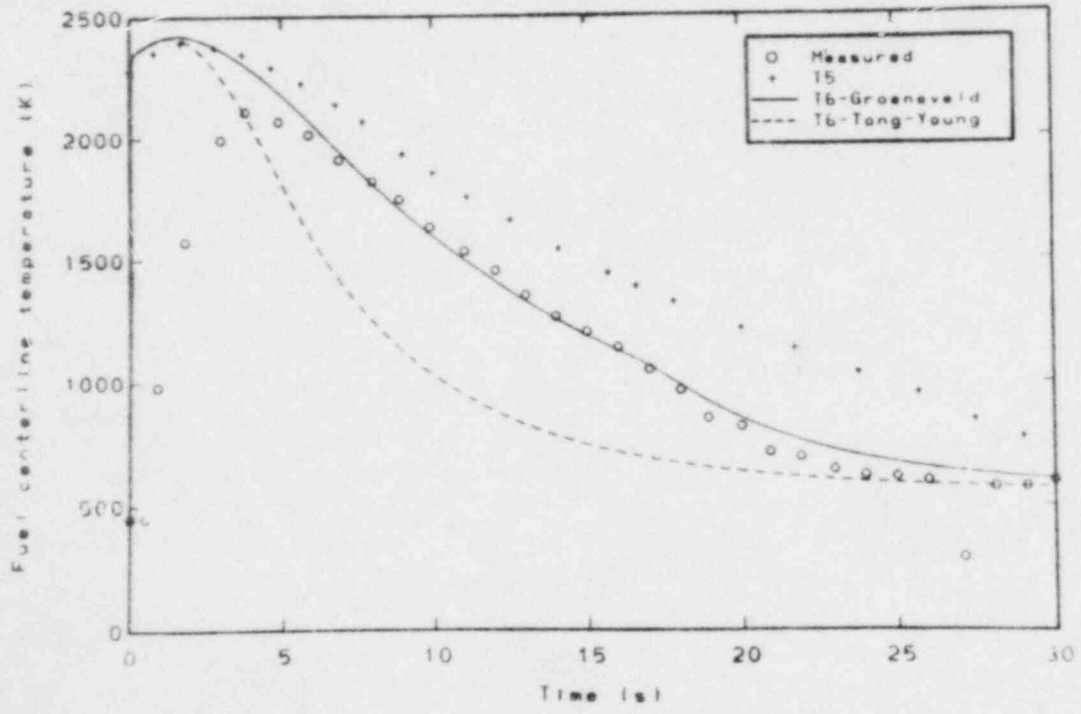

Figure 10. Comparison of measured and calculated fuel centerline temperature versus time for Rod 3 of PBF test RIA 1-1.

duration power burst. The measured centerline temperature rises more slower than the calculated temperature due to the slow response time of the measuring instrumentation. The calculated and measured peak fuel centerline temperatures are 2400 and 2125 K, respectively. Since the slow response time of the measuring instrument results in an underestimation of temperature, the calculated and measured temperatures are considered to be in agreement. The fuel temperature decreased after the power burst due to fuel rod cooling. The FRAP-T6 calculated temperature decrease is in good agreement with the measured temperature decrease. The FRAP-T6 calculated temperatures are significantly improved over the FRAP-T5 calculated temperatures.

A FRAP-T6 computer analysis provides the values of all the variables necessary for a check of energy balance. The code output allows each user to check the modeling of fuel and cladding heat capacity. The variables output by the code include: (a) energy stored in fuel, (b) energy stored in cladding, (c) energy input to fuel rod by fissioning and radioactive decay during a transient, and (d) energy output from fuel rod by cooling during a transient. The change in stored energy during a transient should equal the difference between the energy input and output. The developmental assessment computer analyses have shown that the error in energy balance is less than 1%.

2.2.2 Assessment of the Modeling of Heat Removal. A significant fraction of the energy stored in a fuel rod at the start of a large break LOCA is removed from the fuel rod during the blowdown period. Typically, over 50% of the stored energy is removed. A larger amount of energy removal results in lower cladding temperatures during the reflood period, and conversely, a smaller amount results in higher cladding temperatures during the reflood period. The experimental data of three PBF test rods are used to assess the modeling of energy removal during the blowdown period of a LOCA. The three test rods are Rod 15 of the PCM-4 test,[11] Rod 3 of the LOC-3 test,[12] and Rod 3 of the LOC-11C test.[4] The test fuel rods are typical of 15 by 15 PWR fuel rods. The design characteristics of the test fuel rods are shown in Tables 13, 14 and 1 , respectively.

TABLE 13. CHARACTERISTICS OF ROD 15 OF PBF TEST PCM-4

Characteristic	Value
Fuel Enrichment (wt % U^{235})	20.0
Fuel Density (% Theoretical Density)	93.7
Radial Fuel-Cladding Gap (mm)	0.099
Cladding Thickness (mm)	0.63
Cladding Outside Diameter (mm)	10.76
Fuel Pellet Outside Diameter (mm)	9.30
Fill Gas Composition	Helium
Fill Gas Pressure (MPa)	2.59
Burnup (MWs/kg)	0
Active Fuel Stack Length (m)	0.913
Plenum Volume (mm^3)	5872
Axial Power Peaking Factor	1.36
Cladding Cold Work (%)	10
Diameter of Hole for Thermocouple at Fuel Center	1.86

TABLE 14. CHARACTERISTICS OF ROD 3 OF PBF TEST LOC-3

Characteristic	Value
Fuel Enrichment (wt % U^{235})	12.5
Fuel Density (% Theoretical Density)	94.5
Radial Fuel-Cladding Gap (mm)	0.108
Cladding Thickness (mm)	0.59
Cladding Outside Diameter (mm)	9.93
Fuel Pellet Outside Diameter (mm)	8.53
Fill Gas Composition	He
Fill Gas Pressure (MPa)	4.83
Burnup (MWs/kg)	0
Active Fuel Stack Length (m)	0.879
Plenum Volume (mm^3)	4700
Axial Power Peaking Factor	1.23
Cladding Cold Work (%)	0
Diameter of Hole for Thermocouple at Fuel Center (mm)	1.88

The calculated and measured fuel centerline temperatures for the PCM-4 test are compared in Figure 11. The local fuel rod power at the start of the transient was 51.4 kW/m. The temperature is calculated with both the nonuniform gap and the relocation models for fuel deformation. The temperature is also calculated with the FRAP-T5 code. At the start of the transient, the temperature calculated using the relocation model agrees closely with the measured temperature. After a time of 5 s, however, the calculated temperature is less than the measured temperature. This indicates that the initial stored energy is underpredicted. At the start of the transient, the fuel centerline temperature calculated using the nonuniform gap model is 100 K greater than the measured fuel centerline temperature. After 3 s, the calculated fuel centerline temperature slightly exceeds the measured temperature. At the start of the transient, the temperature calculated by FRAP-T5 is 200 K above the measured temperature. After 5 s, the calculated fuel centerline temperatures agree closely with the measured temperatures.

The calculated and measured fuel centerline temperatures for Rod 3 of the LOC-11C test are compared in Figure 12. The local fuel power at the start of the test was 67.7 kW/m. The fuel centerline temperature is calculated with both the nonuniform gap and the relocation models for fuel deformation. The fuel centerline temperature is also calculated with the FRAP-T5 code. At the start of the transient, the fuel centerline temperatures calculated with both the nonuniform gap model and the relocation model are approximately 120 K less than the measured temperature. At a time of 10 s, the temperature calculated with the relocation model is 90 K less than the measured temperature, while the temperature calculated with the nonuniform gap model agrees closely with the measured temperature. These differences in calculated temperature are due to differences in calculated fuel stored energy. At the start of the transient, a stored energy of 314 kW·s/m is calculated with the relocation model, while a stored energy of 337 kW·s/m is calculated with the nonuniform gap model. At the end of the blowdown period, a stored energy of 186 kW·s/m is calculated with the relocation model, while a stored energy of 193 kW·s/m is calculated with the nonuniform gap model.

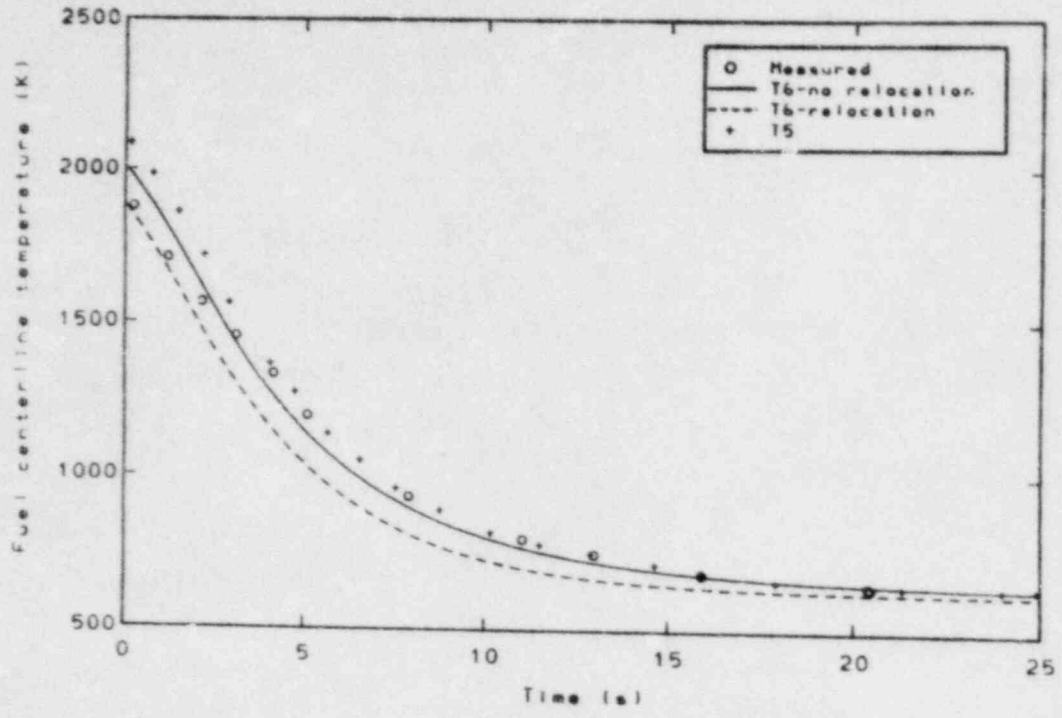

Figure 11. Comparison of measured and calculated fuel centerline temperature versus time for Rod 15 of the PBF test PCM-4.

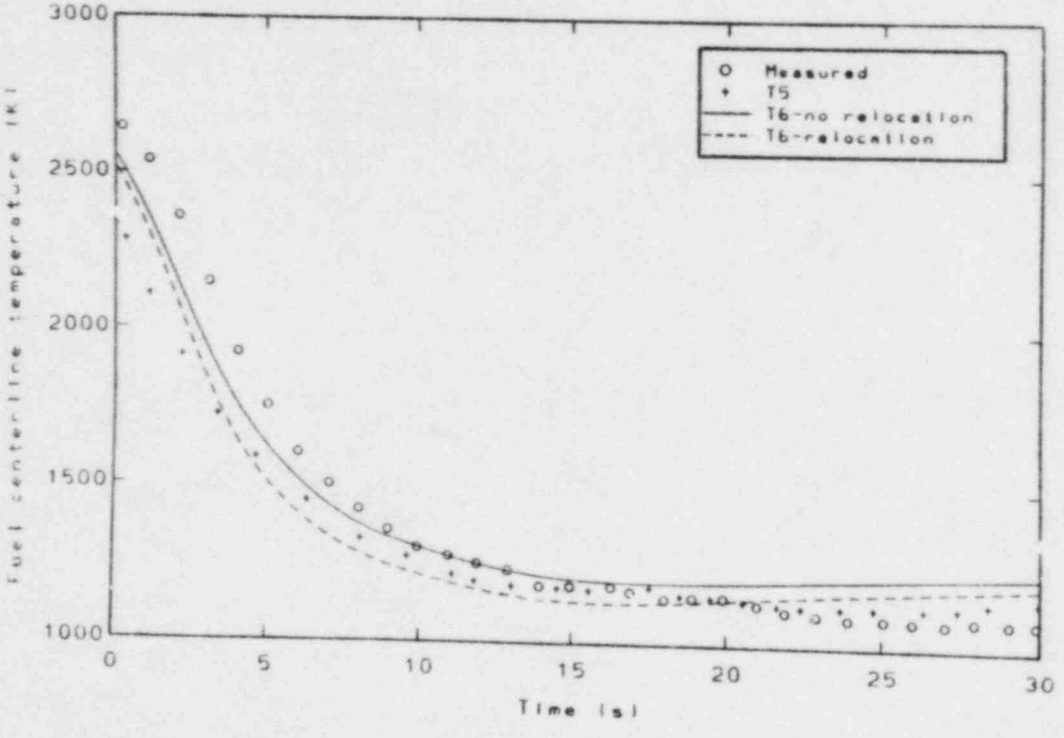

Figure 12. Comparison of measured and calculated fuel centerline temperature versus time for Rod 3 of PBF test LOC-11C.

The calculated and measured fuel centerline temperatures for the LOC-3 test are compared in Figure 13. The local fuel rod power at the start of the test is assumed to be 44.3 kW/m, although the experiment analysis indicates the power to be 55.3 kW/m.[a] The temperature is calculated with both the nonuniform gap and the relocation models for fuel deformation. At the start of the transient, the fuel centerline temperature calculated with the nonuniform gap model is 25 K greater than the measured temperature, while the fuel centerline temperature calculated with the relocation model is 120 K less than the measured temperature. These temperature differences are consistent with the temperature differences observed in Section 2.1.1. A fuel stored

a. A considerable amount of uncertainty is involved in the experimental data used to calculate the fuel rod power. If the local fuel rod power is assumed to be 44.3 kW/m, the difference between the calculated and measured fuel centerline temperature at the start of the test is consistent with the differences observed in Section 2.1.1 for fuel rods similar in design to the LOC-3 test fuel rods.

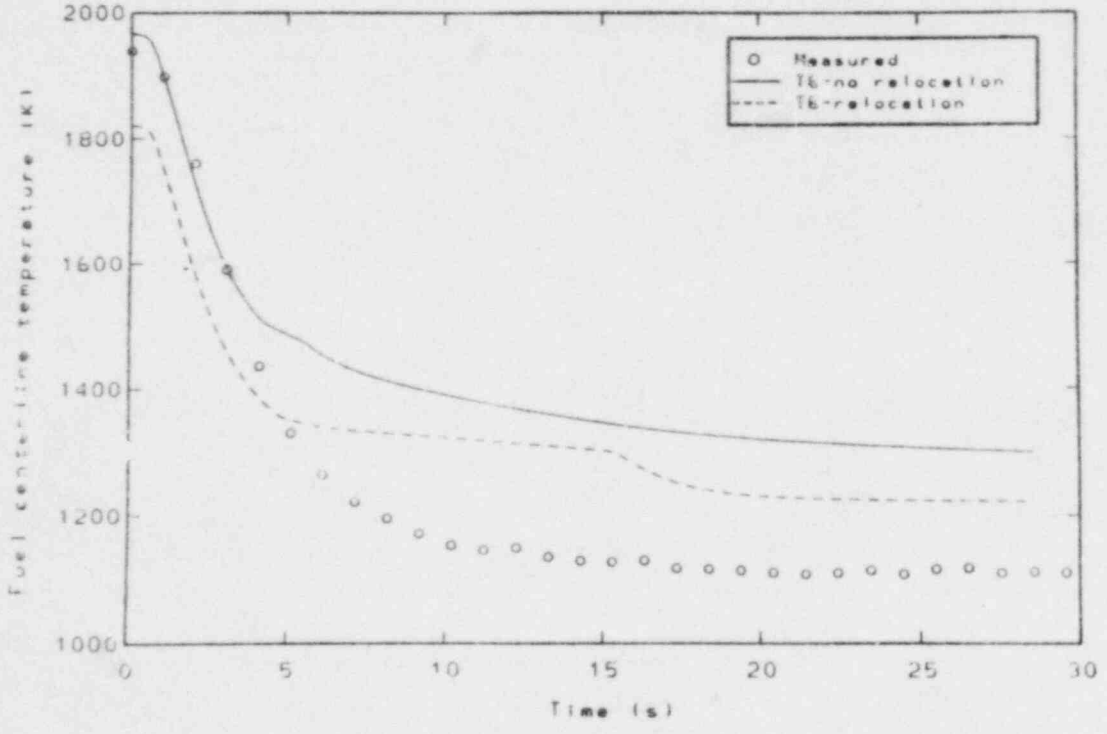

Figure 13. Comparison of measured and calculated fuel centerline temperature versus time for Rod 3 of PBF test LOC-3.

energy of 214·kW s/m is calculated with the nonuniform gap model, while a stored energy of 182 kW·s/m is calculated with the relocation model. After the coolant blowdown begins and the reactor is scrammed, the fuel temperatures calculated with both fuel deformation models decrease in accordance with the measured temperatures. After 5 s, however, the calculated temperatures begin to exceed the measured temperatures. The temperatures calculated with the nonuniform gap model are 200 K greater than the measured temperatures, while the temperatures calculated with the relocation model are 120 K greater than the measured temperatures.

The overestimation of fuel temperature for the last part of the transient is due to an underprediction of fuel rod cooling. As discussed in Section 3, the cooling is underpredicted because the calculated time (0.5 s) for departure from nucleate boiling (DNB) is 1.5 s earlier than the observed time (2.0 s). Because of the error in calculating the time of DNB, the calculated fuel stored energy at the observed time of DNB is about 25% greater than the actual stored energy. The overprediction of stored energy results in a 100 to 200 K overprediction of the fuel temperature.

The effect of the time of DNB upon stored energy is obtained from the calculations for the PCM-4 test. At the start of this test, the reactor was scrammed and complete cooling of the test fuel rod was maintained. DNB did not occur during the transient. The calculated removal of stored energy in the fuel as a function of time is shown in Table 15. The local fuel rod power at the start of the transient is 59 kW/m and the local net fuel stored energy is 200 kW·s/m. During the time interval of 0.5 to 2.0 s, about 25% of the initial stored energy is removed.

The calculations for the LOC-3 test are repeated with the calculated time of DNB forced to equal the observed time of DNB. The calculations are performed with the nonuniform gap model. The calculated and measured fuel centerline temperatures are compared in Figure 14. At a time of 30 s, the calculated temperature is 100 K greater than the measured temperature. This discrepancy is 100 K less than the discrepancy calculated with an uncorrected time of DNB.

TABLE 15. RATE OF REMOVAL OF STORED ENERGY

Time After Reactor Scram (s)	Net Stored Energy in Fuel[a] (kW.s/m)	Ratio of Removed Stored Energy to Initial Net Stored Energy (%)
0	200	0
1.0	164	18
2.0	135	33
3.0	111	45
4.0	91	55
5.0	74	63

a. Net stored energy is equal the total stored energy minus the stored energy at zero power and ambiant coolant conditions (54 kW.s at coolant temperature of 586 K).

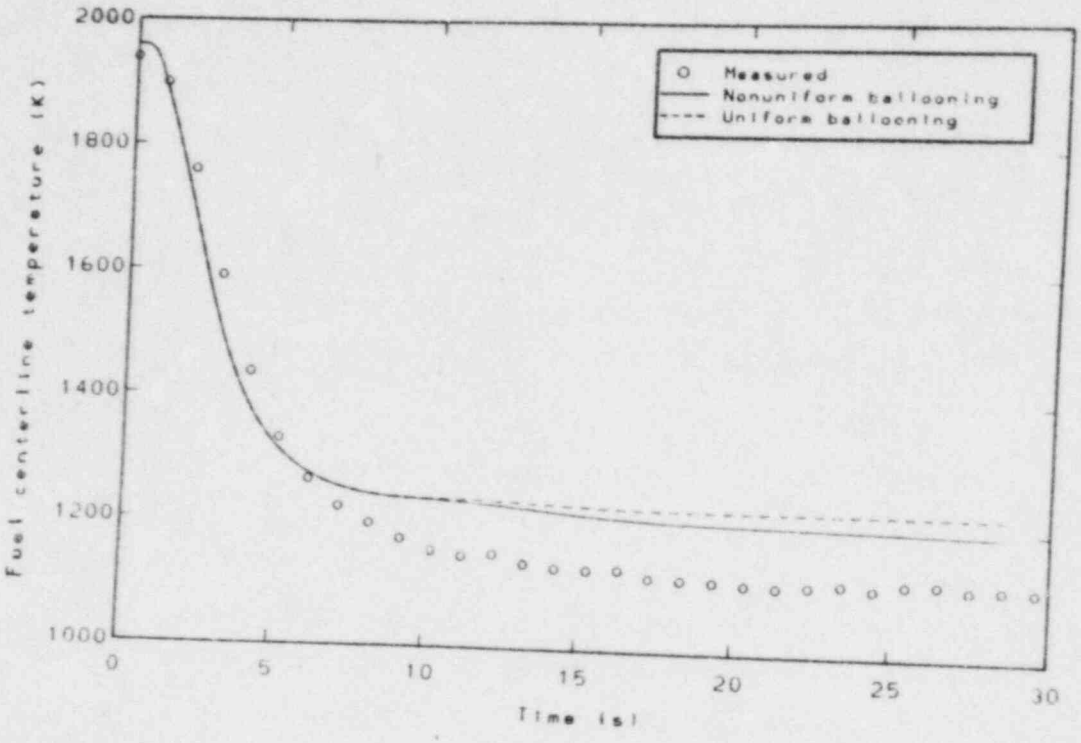

Figure 14. Comparison of measured and calculated fuel centerline temperature versus time for Rod 3 of PBF test LOC-3 (corrected time of DNB).

2.3 Summary and Conclusions

The temperature calculations have been examined by comparisons between calculated and measured fuel temperature. The comparisons have been made for fuel rods typical of commercial reactor fuel rods with low fuel burnup. The calculations were made using both the nonuniform fuel-cladding gap and the relocation models for fuel deformation. The steady state comparisons are presented in Section 2.1 and the transient comparisons are presented in Section 2.2. The results of the comparisons are summarized as follows.

1. The thermal conductivity and heat capacity of the fuel and cladding are accurately modeled. Any errors in the modeling of thermal conductivity and heat capacity contribute to less than a 1% error in the calculation of temperature.

2. For a fuel rod at a power less than 50 kW/m, the fuel-cladding gap conductance is undercalculated by 10 to 20% with the nonuniform fuel-cladding gap model. This leads to a 2% overprediction of fuel temperature for a helium filled fuel rod and a 5 to 10% overprediction of fuel temperature for a xenon filled fuel rod.

3. In a fuel rod at a power less than 50 kW/m, the fuel-cladding gap conductance is overpredicted by a factor of two with the relocation model. This leads to a 5% underprediction of fuel temperature for a helium filled fuel rod and a 15 to 25% underprediction of fuel temperature for a xenon filled fuel rod.

4. For a helium filled fuel rod at a power less than 50 kW/m, the stored energy in the fuel is overpredicted by 0 to 5% with the nonuniform gap model and is underpredicted by 5 to 10% with the relocation model.

5. For a fuel rod power greater than 60 kW/m, the fuel-cladding gap conductance is underpredicted with both the nonuniform gap model and the relocation model. The discrepancy causes the fuel centerline temperature to be underpredicted by 4%. The discrepancy may be due to the simplified modeling of fuel-cladding gap closure. If the fuel-cladding gap is "closed" and the interfacial pressure is greater than zero, both mechanical response models assume a circumferentially uniform gap conductance. In reality, fuel-cladding gaps occur at scattered circumferential locations, which lower the overall fuel-cladding gap conductance.

6. The temperature calculations of the FRAP-T6 code are improved over those of the FRAP-T5 code. For a helium filled fuel rod at a power of 30 kW/m, FRAP-T6 and FRAP-T5 overpredict the fuel centerline temperature by 2% and 5%, respectively.

The following conclusions are drawn from the results of the comparisons between calculated and measured fuel temperature.

1. For the developmental assessment cases, the nonuniform gap model gives better agreement with the experimental data than the relocation model. However, both models are applicable to calculating the steady state and transient temperature and stored energy of BWR and PWR fuel rods. For helium filled fuel rods, the fuel temperature and stored energy calculated with the nonuniform gap model exceed measured values by 0 to 5%. For fuel rods filled with a mixture of helium and xenon, the fuel temperature and stored energy are overpredicted by 5 to 10% using the nonuniform gap model.

2. Using the nonuniform gap model, the temperature calculations of FRAP-T6 are improved over those of FRAP-T5.

3. Using the relocation model for fuel deformation, the temperature and stored energy of BWR and PWR fuel rods are underpredicted by 5 to 10%. To improve the calculation of temperature and

stored energy, the modeling of the fuel-cladding gap conductance should be modified. Currently, the closed gap conductance model is used without regard for the fuel-cladding gap size. Until hard pellet-cladding mechanical interaction occurs, this model should be replaced by the open gap conductance model given a zero fuel-cladding gap size. The fuel-cladding gap conductance calculated by the open gap model given a zero fuel-cladding gap size is 50% of that calculated by the closed gap conductance model given a zero fuel-cladding interfacial pressure. This change in fuel-cladding gap conductance would increase the calculated fuel temperatures and lead to good agreement between calculated and measured temperatures.

3. ASSESSMENT OF CRITICAL HEAT FLUX AND HEAT TRANSFER CORRELATIONS

FRAP-T6 uses heat transfer and critical heat flux correlations to calculate the amount of heat transfer from the surface of a fuel rod to the surrounding coolant. If DNB results, these correlations have a strong influence on the calculated temperature of the fuel rod. The heat transfer correlations relate the cladding surface heat flux to the cladding temperature and the coolant mass flux, quality and pressure. The pre-DNB relation of surface heat flux to cladding temperature is much different than the post-DNB relation, so a different heat transfer correlation is used after DNB than before DNB. The critical heat flux correlations relate the cladding surface heat flux at which DNB occurs to the coolant mass flux, quality and pressure. The critical heat flux correlation determines whether the pre-DNB or post-DNB heat transfer correlation is used.

Several different heat transfer correlations and critical heat flux correlations can be selected by the code user. The assessment of all the correlations exceeds the scope of the developmental assessment effort. The assessment is confined to the correlations that are in FRAP-T6 but not in FRAP-T5. The assessed correlations are the combined Tong-Young and Condie-Bengston heat transfer correlation for high flow film boiling and the combined W-3 and Hsu-Beckner critical heat flux correlation.

The correlations are assessed by comparing the calculated and measured cladding surface temperature for fuel rod tests in which film boiling occurred. The cladding surface temperature is also calculated using the Groeneveld heat transfer correlation and the B&W-2 critical heat flux correlation. These correlations are the standard correlations in FRAP-T5 and are also in FRAP-T6.

A generalized version of the FLECHT correlation is in FRAP-T6 but not in FRAP-T5. The FLECHT correlation calculates the amount of heat transfer from fuel rods to coolant during the reflood period of a LOCA. The correlation has been previously compared with experimental data, so a quantitative assessment is not made in this report. However, the capability of the correlation is demonstrated by a presentation of the calculated cladding surface temperature history for a hypothetical PWR LOCA.

The results of two PBF LOCA tests and two PBF Reactivity Initiated Accident (RIA) tests are used to assess the heat transfer and critical flux correlations. The test rods are Rod 3 of the LOC-11C test, Rod 3 of the LOC-3 test, Rod 3 of the RIA 1-1 test and Rod 2 of the RIA 1-2 [13] test. The design characteristics of the test rod of the RIA 1-2 test are shown in Table 16. The design characteristics of the other fuel rods are shown in Section 2.

The calculations for each test are performed with two different combinations of critical heat flux and heat transfer correlations. The first combination is the W-3 critical heat flux correlation and the combined Tong-Young and Condie-Bengston heat transfer correlation. The second combination is the B&W-2 critical heat flux correlation and the Groeneveld heat transfer correlation.

3.1 PBF Test LOC-11C Cladding Surface Temperature Comparisons

The calculated and measured cladding surface temperatures for Rod 3 of the LOC-11C test are compared in Figure 15. DNB is indicated by a sudden increase in the cladding temperature. The observed time of DNB is 1.5 s. The calculated time for DNB is 1.5 s with the W-3 critical heat flux correlation and 0.05 s with the B&W-2 critical heat flux correlation. After DNB has occurred, the calculations with the combined

TABLE 16. CHARACTERISTICS OF ROD 2 OF PBF TEST RIA 1-2

Characteristic	Value
Fuel Enrichment (wt % U^{235})	12.5
Fuel Density (% Theoretical Density)	94
Radial Fuel-cladding Gap (mm)	0.082
Cladding Thickness (mm)	0.62
Cladding Outside Diameter (mm)	9.99
Fuel Pellet Outside Diameter (mm)	8.59
Fill Gas Composition	77.7% He, 22.3% Ar
Fill Gas Pressure (MPa)	2.41
Burnup (MWs/kg)	0.44×10^6
Active Fuel Stack Length (m)	0.914
Plenum Volume (mm^3)	6455
Axial Power Peaking Factor	1.36
Cladding Cold Work (%)	10

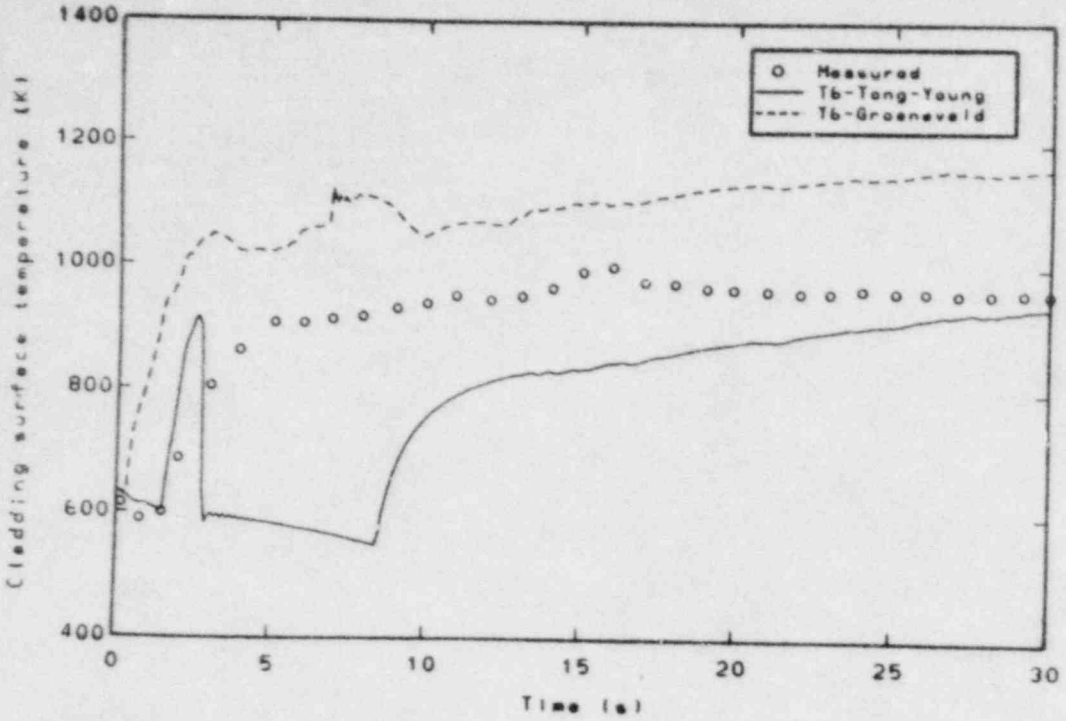

Figure 15. Comparison of measured and calculated cladding surface temperature versus time for Rod 3 of PBF test LOC-11C.

Tong-Young and Condie-Bengston heat transfer correlation overpredict the fuel rod cooling, and cladding rewet is calculated to occur 1.4 s after DNB. After DNB has occurred, the cladding temperature calculated with the Groeneveld correlation is 120 K greater than the measured temperature. This overprediction is due to the discrepancy between the calculated and observed time of DNB. After DNB has occurred and stable film boiling is established, the calculated cladding temperature continues to increase, while the observed cladding temperature remains almost constant. This difference between calculated and measured cladding temperature is because the calculations neglect the radiation heat transfer to the flow shroud.

3.2 PBF Test LOC-3 Cladding Surface Temperature Comparisons

The calculated and measured cladding surface temperatures for Rod 3 of the LOC-3 test are compared at elevations of 0.625 m and 0.675 m. The temperature comparisons are shown in Figures 16 and 17, respectively. The W-3 and B&W-2 correlations both calculate DNB to occur at about the same time. At the 0.625 m elevation, the calculated time of DNB is 0.5 s, while the observed time is 2.0 s. At the 0.675 m elevation, the calculated

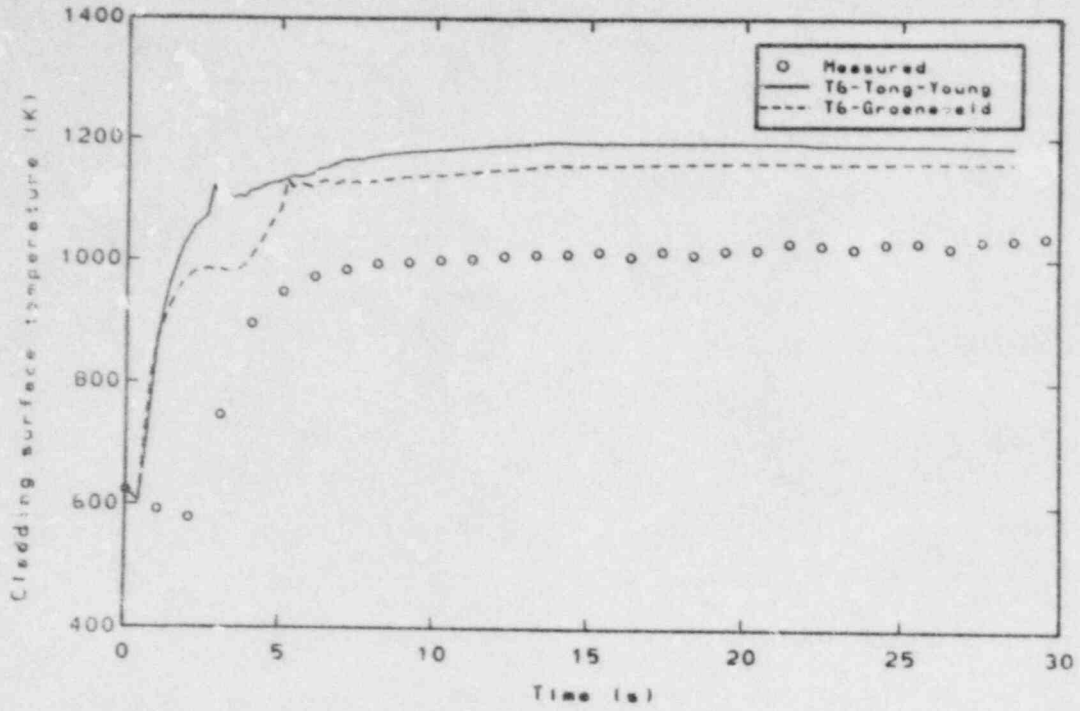

Figure 16. Comparison of measured and calculated cladding surface temperature versus time at the 0.625 m elevation for Rod 3 of PBF test LOC-3.

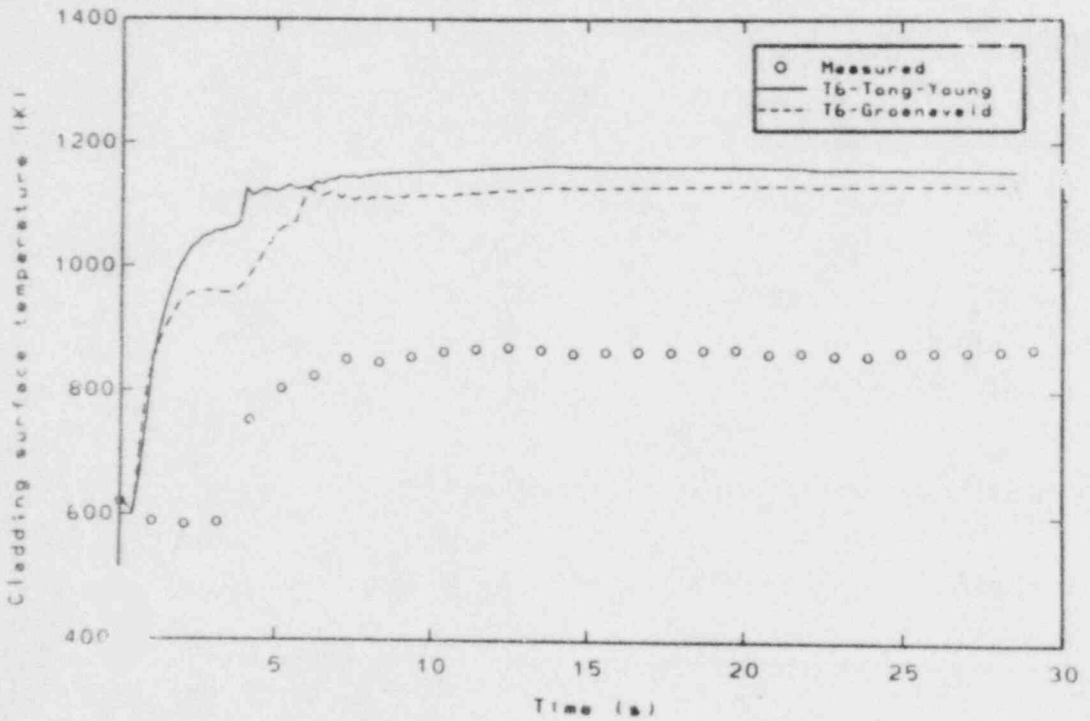

Figure 17. Comparison of measured and calculated cladding surface temperature versus time at the 0.675 m elevation for Rod 3 of PBF test LOC-3.

time of DNB is 0.4 s, while the observed time is 3.1 s. The post-DNB calculated cladding temperature is about the same using either the Tong-Young or the Groeneveld correlations.

The calculated post-DNB cladding temperature is greater than the measured temperature because of the discrepancy between the calculated and observed time of DNB. At the 0.625 m elevation, where the calculated time of DNB is 1.5 s earlier than the observed time of DNB, the calculated temperature is 200 K greater than the measured temperature. At the 0.675 m elevation, where the calculated time of DNB is 2.7 s earlier than the observed time, the calculated temperature is 300 K greater than the measured temperature.

The calculations for the LOC-3 test are repeated with the calculated time of DNB forced to equal the observed time of DNB.[a] The calculations are performed with the nonuniform gap model and the Groeneveld heat transfer correlation. The calculated and measured cladding temperature at the 0.625 m elevation are compared in Figure 18. After DNB has occurred, the calculated cladding temperature is about 60 K greater than the measured temperature. The cladding temperature calculated with an uncorrected time of DNB is 200 K greater than the measured temperature. The calculated and measured cladding temperatures at the 0.675 m elevation are compared in Figure 19. The calculated and measured cladding temperatures are within 20 K of each other. The cladding temperatures calculated with an uncorrected time of DNB are 300 K greater than the measured temperatures.

3.3 PBF Test RIA 1-2 Cladding Surface Temperature Comparisons

The calculated and measured cladding surface temperatures for Rod 2 of the RIA 1-2 test are compared at elevations of 0.454 m (power Peak) and 0.74 m. The temperature comparisons are shown in Figures 20 and 21, respectively. Both the calculations and the measurements show that DNB occurs immediately after the power bur

---

a. The "SPECIFIED FBZ" suboption of the "COOLANT CONDITION" option is used, which allows the code user to prescribe the time of film boiling.

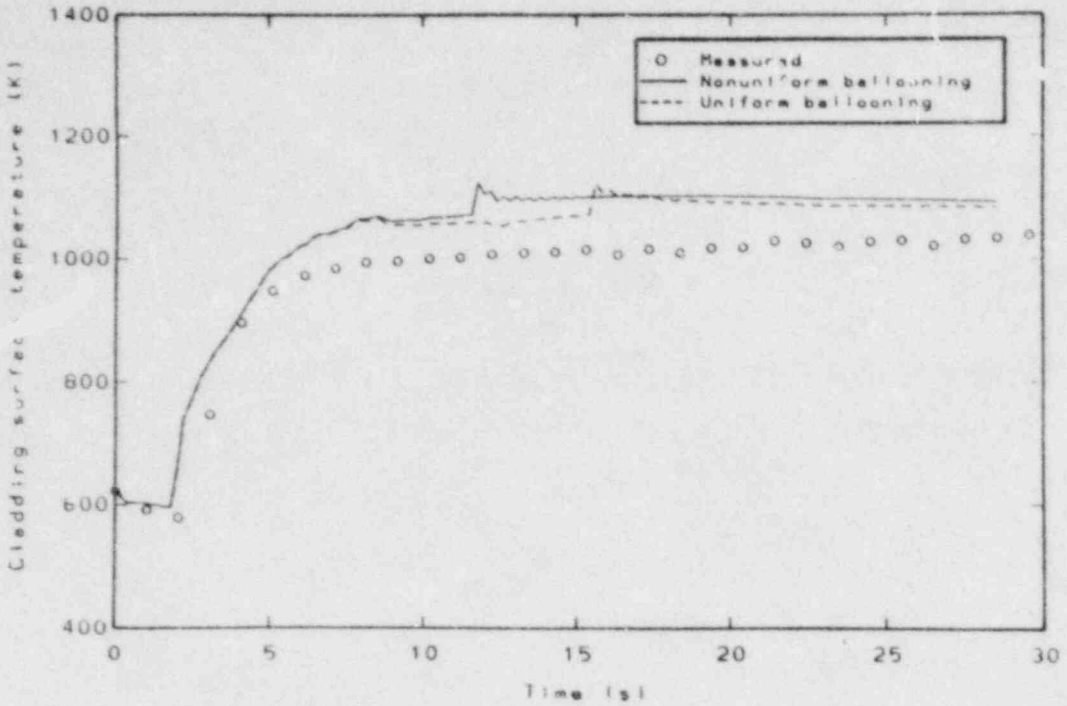

Figure 18. Comparison of measured and calculated cladding surface temperature versus time at the 0.625 m elevation for Rod 3 of PBF test LOC-3 (corrected time of DNB).

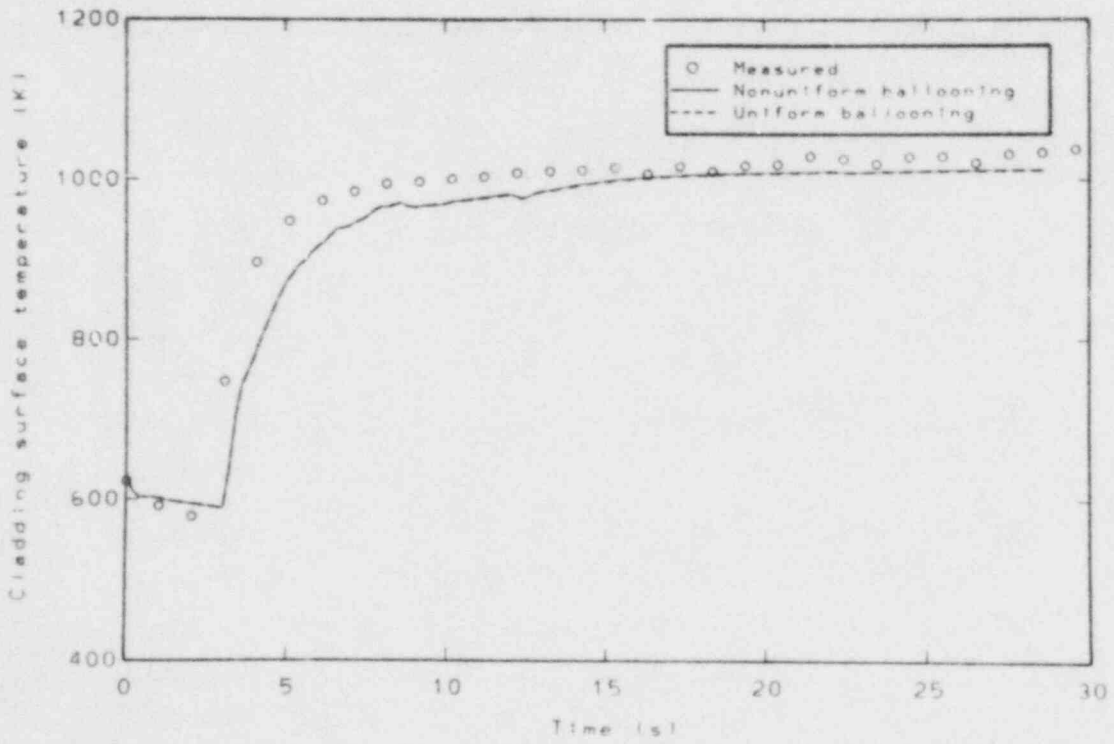

Figure 19. Comparison of measured and calculated cladding surface temperature versus time at the 0.675 m elevation for Rod 3 of PBF test LOC-3 (corrected time of DNB).

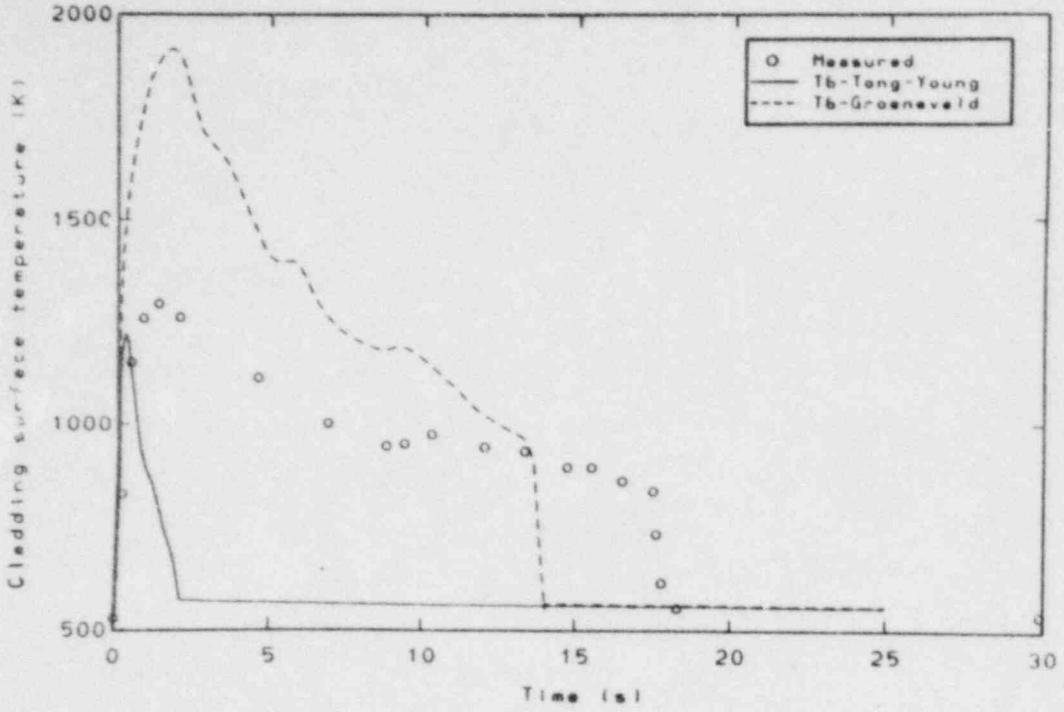

Figure 20. Comparison of measured and calculated cladding surface temperature versus time at the 0.454 m elevation for Rod 2 of PBF test RIA 1-2.

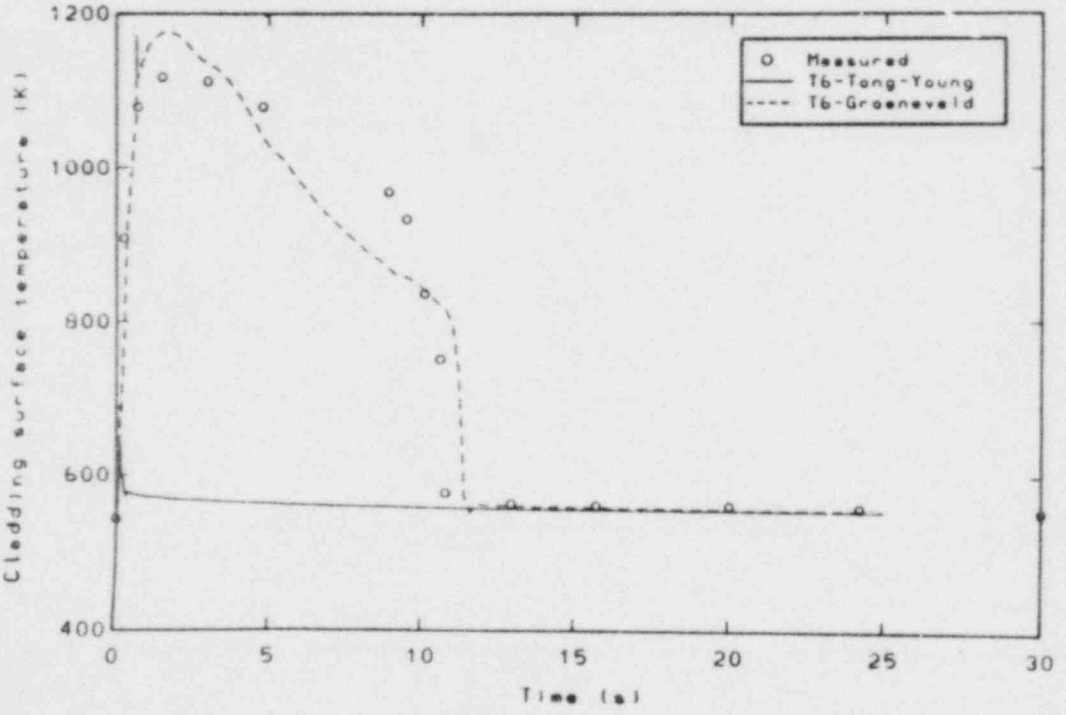

Figure 21. Comparison of measured and calculated cladding surface tmeperature versus time at the 0.79 m elevation for Rod 2 of PBF test RIA 1-2.

At the 0.454 m elevation, the peak measured cladding temperature is 1300 K. A peak temperature of 1230 K is calculated using the Tong-Young correlation, and a peak temperature of 1400 K is calculated using the Groeneveld correlation. The observed time of cladding rewet is 18 s. A rewet time of 2.5 s is calculated using the Tong-Young correlation and a rewet time of 14 s is calculated using the Groeneveld correlation.

At the 0.79 m elevation, the cladding temperature calculated using the Groeneveld correlation agrees closely with the measured temperature. Both the peak cladding temperature and the time of cladding rewet are correctly calculated. With the Tong-Young correlation, however, cladding rewet is calculated to occur shortly after DNB has occurred.

3.4 PBF Test RIA 1-1 Cladding Surface Temperature Comparisons

The calculated and measured cladding surface temperatures for Rod 3 of the RIA 1-1 test are compared in Figure 22. The temperature is calculated using both the FRAP-T5 and FRAP-T6 codes. For the FRAP-T5 calculation, the Groeneveld heat transfer correlation is used. The FRAP-T6 calculation is performed using both the Tong-Young and Groeneveld correlations. The calculations and measurements show that DNB occurs immediately after the power burst. A considerable variance is shown between the calculated peak cladding temperature and measured peak cladding temperature. The measured peak cladding temperature is 1430 K, while the calculated peak cladding temperatures are 1640 K (FRAP-T5), 1600 K (FRAP-T6 with Groeneveld correlation) and 830 K (FRAP-T6 with Tong-Young correlation). A considerable variance is also shown between the calculated and measured time of cladding rewet. The observed time of cladding rewet is 15 s, while the calculated times of cladding rewet are 22 s (FRAP-T5), 16 s (FRAP-T6 with Groeneveld correlation), and 3 s (FRAP-T6 with Tong-Young correlation). Overall, the comparisons show that the cladding temperature is best calculated by FRAP-T6 using the Groeneveld heat transfer correlation.

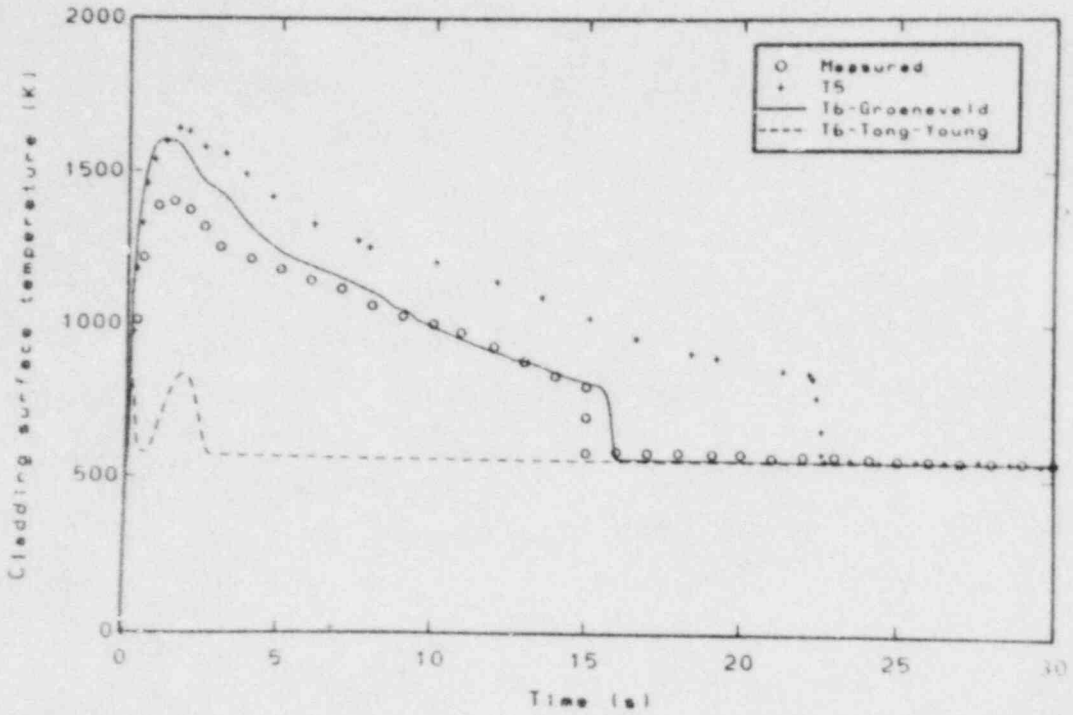

Figure 22. Comparison of measured and calculated cladding surface temperature versus time for Rod 3 of PBF test RIA 1-1.

3.5 Cladding Temperature During a PWR LOCA

The cladding temperature history during a hypothetical large break LOCA in a PWR with 15 by 15 fuel rod bundles is calculated to demonstrate the capability of the generalized FLECHT correlation. An assessment of the correlation with respect to experimental data has been previously made. The hypothetical LOCA is assumed to be caused by a 200% break in the cold leg of the primary coolant loop. Reflooding of the reactor core is assumed to begin 40 s after the initiation of the LOCA. The flooding rate varies from 289 mm/s at the beginning of reflooding to 25 mm/s at the completion of reflooding. The response is calculated of a beginning-of-life fuel rod at an average linear power of 36 kW/m. The fuel rod cooling during the blowdown period is calculated using both the Tong-Young (case 1) and Groeneveld (case 4) heat transfer correlations. The calculated cladding temperature histories at several axial nodes are shown in Figure 23. The elevation of each axial node is given in Table 17. The peak cladding temperature occurs at an elevation of 2.32 m. The peak cladding temperature is 990 K when using the Tong-Young correlation and 1160 K when using the Groeneveld correlation.

3.6 Summary and Conclusions

The critical heat flux and heat transfer correlations have been examined by comparison of calculated and measured cladding temperatures during fuel rod tests in which film boiling occurred. The comparisons are presented in Sections 3.1 through 3.5. The results of the comparisons are summarized as follows.

1. For a LOCA and RIA, the film boiling heat transfer coefficient is underpredicted by 0 to 10% with the Groeneveld correlation.
2. For a LOCA, the film boiling heat transfer coefficient is overpredicted by 0 to 20% with the combined Tong-Young and Condie-Bengston correlation.
3. The combined Tong-Young and Condie-Bengston correlation is not applicable to a RIA.

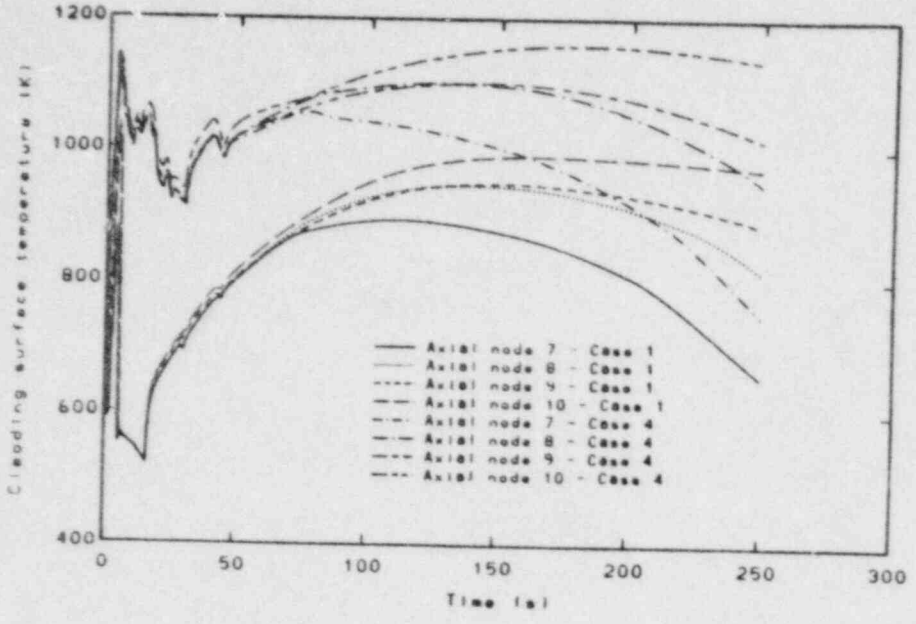

Figure 23. Calculated cladding surface temperature versus time at various axial nodes for a hypothetical LOCA using Tong-Young (case 1) and Groeneveld (case 4) heat transfer correlations.

TABLE 17. ELEVATION OF AXIAL NODES FOR PWR LOCA PROBLEM

Axial Node	Elevation Above Bottom of Fuel Stack (m)
7	1.58
8	1.83
9	2.07
10	2.32

4. For a large break LOCA test in PBF, the time of DNB is calculated to occur earlier than the observed time. The time of DNB calculated with the B&W-2 critical heat flux correlation is 1 to 3 s earlier than the observed time. The time of DNB calculated with the combined W-3 and Hsu-Beckner correlation is 0 to 3 s earlier than the observed time. The best agreement between calculation and observation is obtained with the combined W-3 and Hsu-Beckner correlation.

5. For a large break LOCA, the time at which DNB occurs has a strong influence on the post-DNB cladding temperature. A difference of 1.5 s in the time of DNB leads to a 100 to 150 K difference in the post-DNB cladding temperature.

The following conclusions are drawn from the results presented in Section 3.

1. The FRAP-T6 code is applicable to calculating the transient temperature of fuel rods during a LOCA or a RIA.

2. The Groeneveld correlation provides the best estimate of the high flow film boiling heat transfer coefficient. The combined W-3 and Hsu-Beckner correlation provides the best estimate of the critical heat flux. Using the Groeneveld and combined W-3 and Hsu-Beckner correlations, FRAP-T6 calculates post-DNB fuel rod temperatures that are 0 to 20% greater than measured values.

3. For large break LOCA tests in PBF, FRAP-T6 calculates DNB to occur 1 to 3 s earlier than observed. An error of just 1.5 s in the calculation of time of DNB leads to a 10% error in the calculation of the post-DNB fuel rod temperatures. Further investigation should be performed to determine the reason for the disagreement between calculated and observed time of DNB. One possible reason is that the critical heat flux correlations in FRAP-T6 were developed from tests on rod bundles, while the test fuel rods of PBF are surrounded with fluted flow shrouds.

4.0 ASSESSMENT OF CLADDING BALLOONING MODELS

The cladding ballooning models calculate the amount of cladding ballooning a fuel rod may experience during a hypothetical LOCA. The models also calculate whether or not the cladding has ruptured due to ballooning.

Cladding ballooning results from a combination of cladding temperature increase and cladding differential pressure increase. The former event weakens the cladding and the latter event increases the load on the cladding. The cladding hoop strain is a measure of the amount of cladding ballooning.

The experimental data of two fuel rod tests are used to assess the cladding ballooning models. The tests are the TREAT FRF-2 test and the PBF LOC-3 test. Cladding ballooning to failure occurred during the two tests. The design characteristics of the test fuel rods have been previously shown in Tables 11 and 14, respectively.

The cladding ballooning models are assessed by comparing calculated and measured fuel rod gas pressures. Since the gas pressure and gas volume are reciprocally related, a correct calculation of the gas pressure indicates a correct calculation of the gas volume and the amount of cladding ballooning. This comparison allows an assessment of both the timing and amount of calculated ballooning. The cladding ballooning models are also assessed by comparing the calculated and measured post-test diameters of the test fuel rod. This comparison allows an assessment of the final shape and magnitude of calculated ballooning.

Cladding ballooning can be calculated using two different models. The code user selects the model to be used. In the first model, the default option, the cladding temperature and ballooning are calculated with BALON2. A 1% circumferential temperature variation is assumed, taking into account the temperature variation of the fuel surface. In the second model, the "NO BALLOON" option, the cladding temperature is assumed to be circumferentially uniform. The cladding ballooning is calculated by FRACAS-I.

4.1 TREAT Test FRF-2 Comparison

Calculated and measured cladding ballooning are compared for Rod 12 of the TREAT FRF-2 test. Rod 12 had no fuel burnup, but was pressurized to 0.5 MPa to simulate an end-of-life BWR fuel rod with no initial pressurization. The test rod instrumentation included a pressure transducer and a thermocouple on the cladding surface. The test fuel rod was subjected to conditions typical of those immediately following the blowdown period of a LOCA. The test rod ballooned and ruptured.

The transient performance of the test rod is calculated using the nonuniform gap model for fuel deformation and bypassing the cladding oxidation model. The calculated and measured cladding temperatures are in good agreement, as shown in Figure 9.

The calculated and measured fuel rod internal gas pressures are compared in Figure 24. From 0 to 25 s, the measured gas pressure increases from 0.77 to 1.0 MPa because of the increase in temperature of the gas. From 0 to 14 s, the calculated gas pressure is in good agreement with the measured gas pressure. From 14 to 15 s, the calculated gas pressure decreases, which indicates that plastic deformation of the cladding is calculated to begin. The cladding temperature is about 750 K at beginning of calculated plastic deformation. At 25 s, the gas pressure begins to decrease in response to the beginning of cladding ballooning. The calculated and observed times for the beginning of cladding ballooning are in good agreement. At 32 s, the measured gas pressure decreases abruptly to the value of the coolant pressure, which indicates that cladding rupture occurred. At the time and elevation of cladding rupture, the cladding is in the beta phase (temperature of 1450 K). A rupture time of 32 s is calculated using the BALON2 model (nonuniform ballooning) and a rupture time of 36 s is calculated using the FRACAS-I model (uniform ballooning). The calculated probability of cladding failure is 0.40 at 32 s (observed time of failure) and 0.52 at 33 s. Between the time cladding ballooning begins (25 s) and the time of cladding rupture (32 s), the calculated and measured gas pressures are in good agreement, which indicates that the rate of cladding ballooning is accurately calculated.

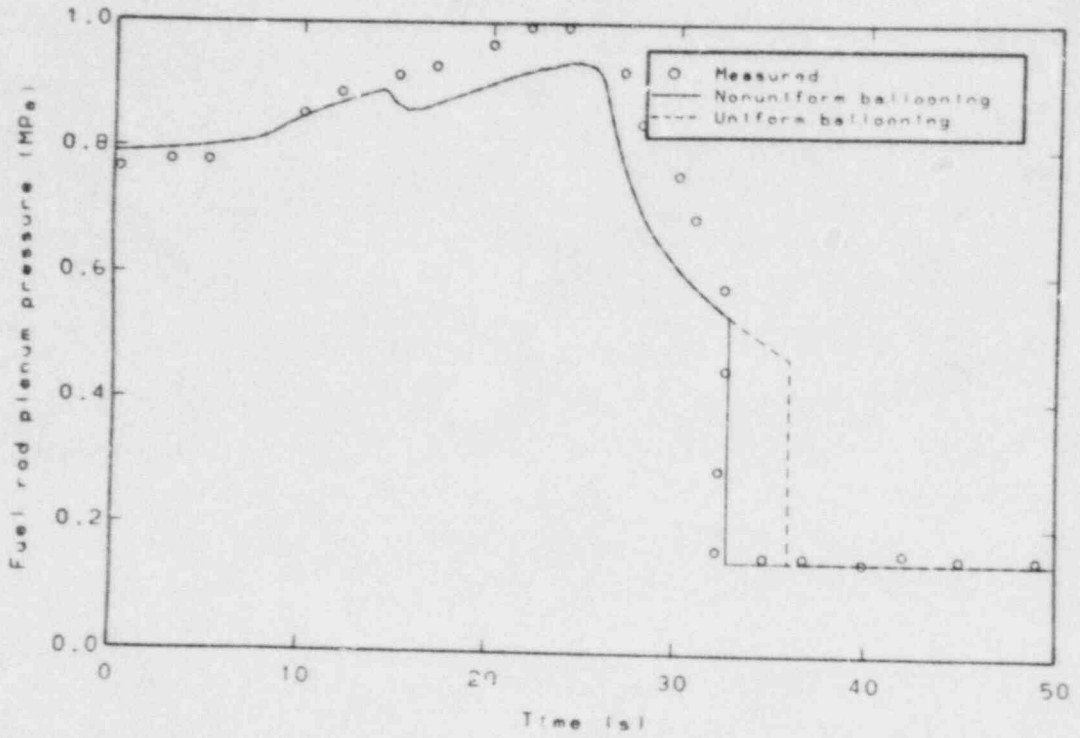

Figure 24. Comparison of measured and calculated fuel rod plenum pressure versus time for Rod 12 of TREAT test FRF-2.

The calculated and measured post-test permanent hoop strains of the cladding are compared in Figure 25. The measured permanent hoop strain varies from less than 1% at the ends of the fuel rod to 60% in the center region where the cladding ruptured. A rupture strain of 43% is calculated using the BALON2 model (nonuniform ballooning) and a rupture strain of 26% is calculated using the FRACAS-I model (uniform ballooning). At the ends of the fuel rod, the calculated permanent hoop strains are greater than the measured permanent hoop strains.

4.2 PBF Test LOC-3 Comparison

The calculated and measured cladding ballooning are compared for Rod 3 of the PBF LOC-3 test. Rod 3 had no fuel burnup, but was highly pressurized (4.83 MPa) to simulate an end-of-life PWR fuel rod. The test rod instrumentation included a pressure transducer, a thermocouple at the fuel center, and thermocouples on the cladding surface at two elevations. The test rod was subjected to power and coolant conditions typical of a large break LOCA. The test rod ballooned and ruptured during the blowdown period of the test.

The transient performance of the test rod is calculated using the models that result in the best calculation of cladding temperature -- the nonuniform gap model and the Groeneveld heat transfer correlation. The time of DNB is corrected to match the observed time of DNB. As previously shown in Figures 18 and 19, these models and corrections produce a calculated cladding temperature that is in approximate agreement with the measured cladding temperature. A good agreement between calculated and measured cladding temperature allows an unbiased assessment of the cladding ballooning calculations.

The calculated and measured fuel rod internal gas pressures are compared in Figure 26. From 0 to 2 s, the measured gas pressure decreases from 15 to 14 MPa because of cooling of the fuel rod. The calculated and measured pressure are in good agreement. At 2 s, DNB occurs, and the cladding temperature increases sharply. Between 2 and 3 s, the measured

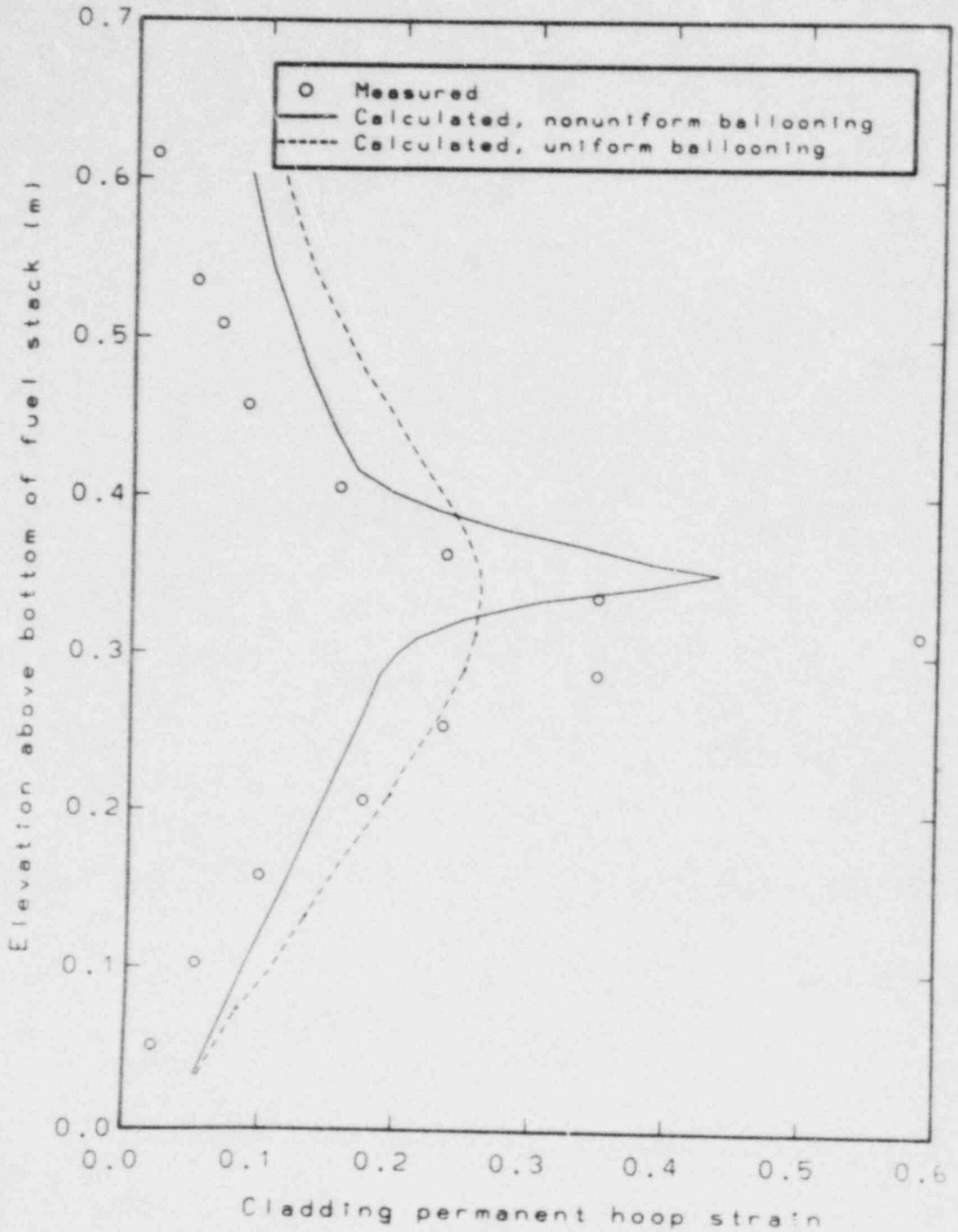

Figure 25. Comparison of measured and calculated cladding permanent hoop strain versus axial elevation for Rod 12 of TREAT test FRF-2.

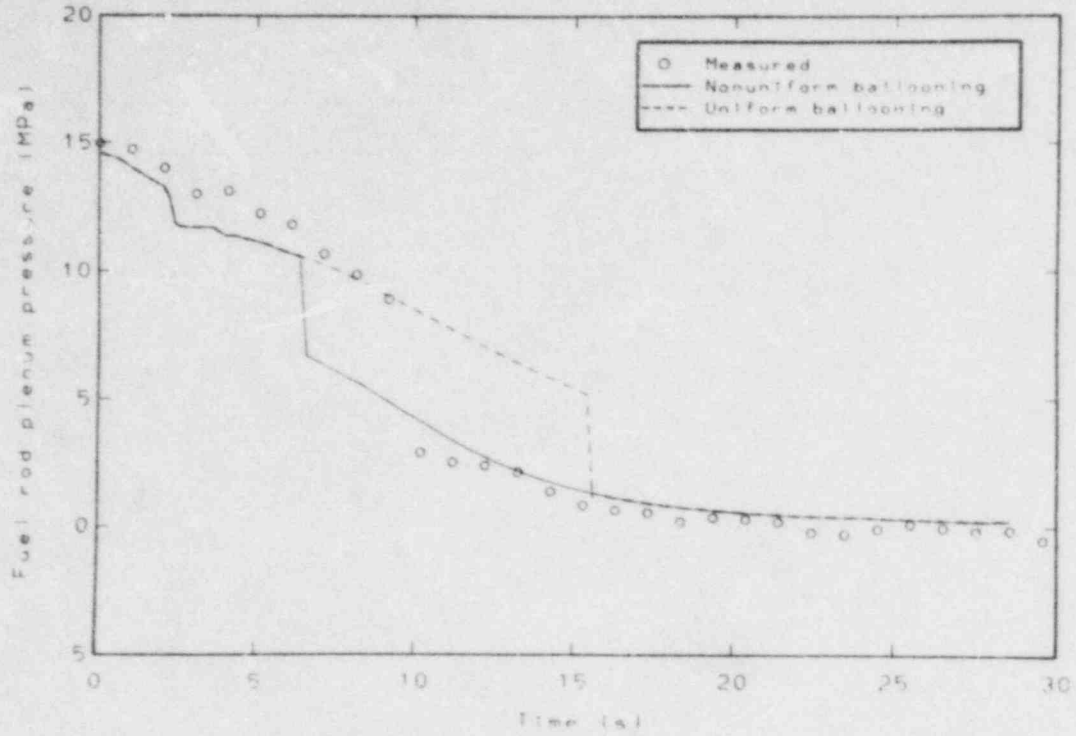

Figure 26. Comparison of measured and calculated fuel rod plenum pressure versus time for Rod 3 of PBF test LOC-3.

gas pressure decreases slightly, which indicates the beginning of plastic deformation of the cladding. During the same interval of time, the calculated pressure also decreases, but the calculated pressure decrease is greater than the measured pressure decrease. Evidently, plastic deformation is calculated to begin at the same time as observed, but the amount of plastic deformation is overcalculated. From 4 to 10 s, the measured gas pressure decreases because of ballooning of the cladding. Beginning at 4 s, the calculated gas pressure also decreases because of cladding ballooning. At 10 s, the measured gas pressure drops sharply to the value of the coolant pressure, which indicates that cladding rupture occurred. At the time and elevation of rupture, the cladding is calculated to be in the alpha to beta transition phase (temperature of 1110 K). A rupture time of 7 s is calculated using the BALON2 model (nonuniform ballooning) and a rupture time of 16 s is calculated using the FRACAS-I model (uniform ballooning). At the time of observed cladding rupture (10 s), the cladding failure probability is calculated to be 0.53 for the calculations using the FRACAS-I model.

The calculated and measured post-test permanent hoop strain of the cladding are compared in Figure 27. The measured permanent hoop strain varies from 0% at the ends of the fuel rod to 23% at the elevation

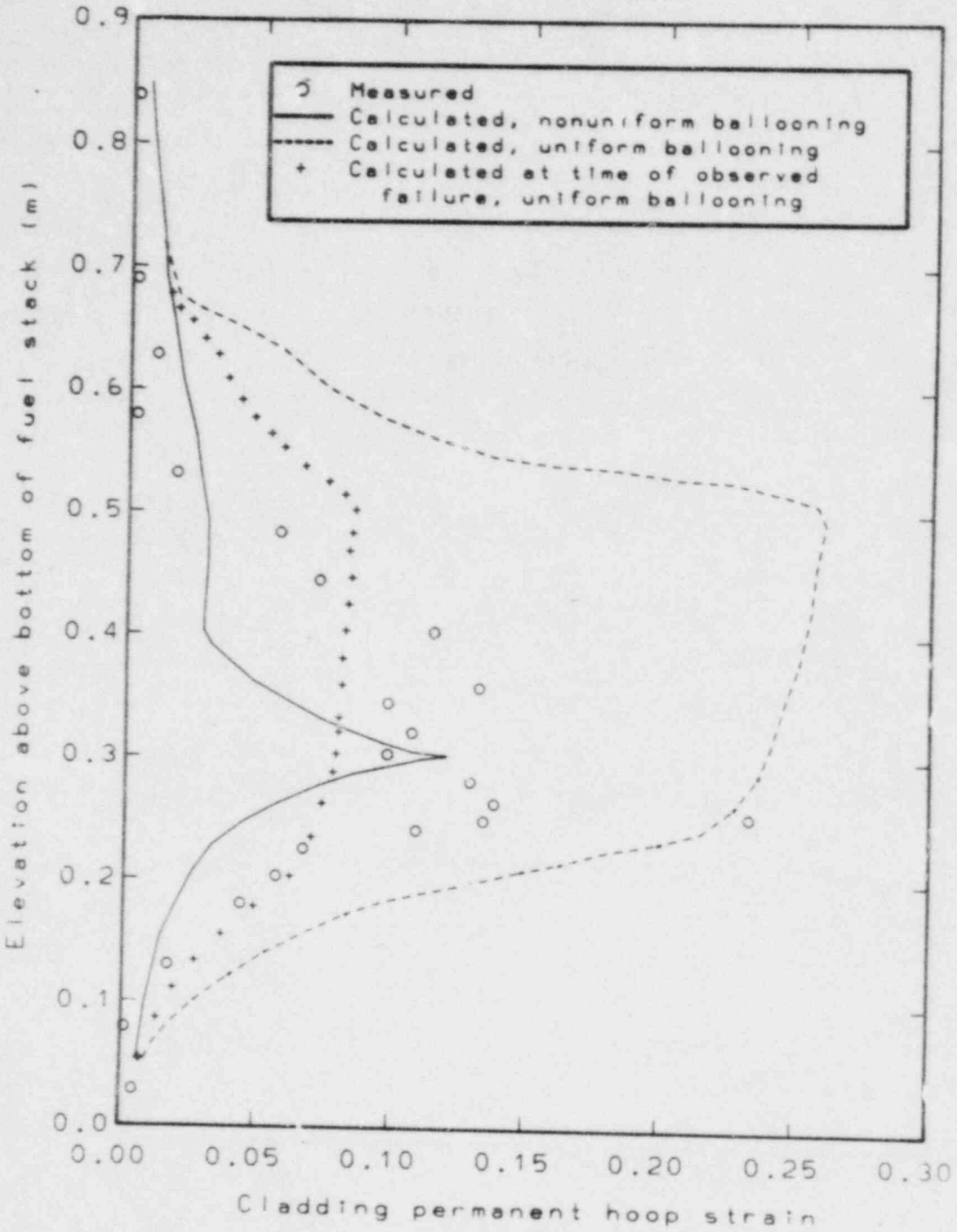

Figure 27. Comparison of measured and calculated cladding permanent hoop strain versus axial elevation for Rod 3 of PBF test LOC-3.

of cladding rupture, which is 0.25 m. Using the BALON2 model (nonuniform ballooning), the calculated peak permanent hoop strain is 13% and the calculated elevation of cladding rupture is 0.30 m. The calculated permanent hoop strains are about 50% of the measured permanent hoop strains because cladding rupture is calculated to occur 3 s sooner than observed. Using the FRACAS-I model, the calculated peak permanent hoop strain is 26% and the calculated elevation of cladding rupture is 0.50 m. Except at the observed elevation of cladding rupture, the calculated permanent hoop strains are about 300% greater than the measured permanent hoop strains. The calculated cladding permanent hoop strains are greater than the measured permanent hoop strains because cladding rupture is calculated to occur 6 s later than observed. At the observed time of cladding rupture, however, the calculated permanent hoop strains are in approximate agreement with the measured permanent hoop strains.

The undercalculation of the cladding permanent hoop strains using the BALON2 model is considered to be due to a slight overcalculation of the cladding temperature. During the period of cladding ballooning, the calculated cladding temperatures are about 50 K greater than the measured temperatures, as shown in Figure 18. The cladding is calculated to be in the alpha to beta transition phase. If the calculated cladding temperatures are about 50 K lower, the cladding is calculated to be in the alpha phase. This results in a later time of rupture and larger final cladding permanent hoop strains.

4.3 Summary and Conclusions

The cladding ballooning models have been assessed by comparisons with experimental data of fuel rod tests in which cladding rupture occurred. The cladding ruptures occurred while the cladding was in either the alpha to beta transition phase (at a temperature between 1090 K and 1250 K) or the beta phase (temperature greater than 1250 K). Cladding ballooning is calculated using both the BALON2 model (nonuniform ballooning) and the FRACAS-I model (uniform ballooning). The calculated and measured fuel rod internal gas pressures are compared and the final calculated and measured cladding permanent hoop strains are compared. The results of the comparisons are summarized as follows.

1. Using the BALON2 model, the time of cladding rupture is accurately calculated for cladding in the beta phase and is approximately calculated for cladding in the alpha to beta transition phase. The calculated cladding rupture strain is about 75% of the measured rupture strain.

2. Using the FRACAS-I and cladding failure probability models (FRAIL), the time of cladding rupture is accurately calculated. The calculated peak cladding permanent hoop strain is about 40% of the measured rupture strain. Away from the 60 mm long region of cladding rupture, the cladding permanent hoop strains are accurately calculated.

3. At the onset of cladding plastic deformation, plastic deformation is calculated to occur faster than observed.

The following conclusions are drawn from the results of the comparisons between calculated and observed cladding ballooning.

1. The cladding ballooning calculations are in approximate agreement with the measurements of fuel rod tests. Calculations using the BALON2 model can be expected to provide the most accurate prediction of cladding permanent hoop strains.

2. The yield stress of the cladding is accurately calculated, but the stress-strain relation in the vicinity of the yield point underpredicts the dependence of stress on strain.

3. Cladding ballooning is strongly influenced by cladding temperature. A thorough quantitative assessment of cladding ballooning models cannot be performed until results of in-pile fuel rods tests with complete measurement of the cladding temperatures are available.

5. ASSESSMENT OF THE FISSION GAS RELEASE MODEL

The fission gas release model, FASTGRASS, calculates the production and release of the noble fission gases. The calculations of the model are important because released fission gases decrease the fuel-cladding gap conductance and increase the fuel rod internal gas pressure. A decreased fuel-cladding gap conductance leads to an increased fuel temperature, which in turn leads to a greater release of fission gases.

5.1 PBF Test IE-3 Comparisons

The experimental data of Rod 17 of the PBF IE-3 test[14] are used to assess the FRAP-T6 fission gas release model. The design characteristics of the test fuel rod are shown in Table 18. The test fuel rod was irradiated in the Saxton reactor to a fuel burnup of 1.28×10^6 MW·s/kg at a rod average power of 30 kW/m. The test fuel rod was then fitted with a pressure transducer to measure the internal gas pressure and placed in a PBF test assembly. During the preconditioning phase of the PBF testing, the test fuel rod was subjected to four power cycles. The duration of the power cycles ranged from two to five hours. The average rod power ranged from 20 to 35 kW/m. The test fuel rod was then subjected to high power steady state operation for one hour. The average fuel rod power was 55 kW/m. The fuel centerline temperature in the region of peak power (76 kW/m) approached the melting temperature, resulting in a significant release of fission gases. The internal pressure increased about 8% due to the release of the fission gases, which indicated that 0.5×10^{-3} moles of fission gas were released during the high power operation.[15]

The performance of the test fuel rod during the Saxton irradiation and the PBF testing is calculated by the FRAP-T6 code using the FASTGRASS model. The code calculates that 0.011 moles of fission gas are produced and 0.0017 moles are released during the Saxton irradiation. The code calculates that 0.0016 moles of fission gas are released during the high power steady state operation of the PBF testing. Most of the fission gas release was calculated to occur during the first 100 s of high power operation. The calculated amount of fission gas release is a factor of three larger

TABLE 18. CHARACTERISTICS OF ROD 17 OF PBF TEST IE-3

Characteristic	Value
Fuel Enrichment (wt % U^{235})	12.5
Fuel Density (% Theoretical Density)	44.4
Radial Fuel-Cladding gap (mm)	0.071
Cladding Thickness (mm)	0.587
Cladding Outside Diameter (mm)	9.85
Fuel Pellet Outside Diameter (mm)	8.53
Fill Gas Composition	Helium
Fill Gas Pressure (MPa)	2.68
Burnup (MWs/kg)	0-1.28 x 10^6
Active Fuel Stack Length (m)	0.904
Plenum Volume (mm^3)	4638
Axial Power Peaking Factor	1.40
Cladding Cold Work (%)	10

than the measured amount of release.

Two assumptions in the calculations contribute to the overprediction of the fission gas release. The first assumption is that no fission gases are released from the fuel during the preparation of the test fuel rod for PBF testing. During the preparation, all of the released fission gases were evacuated and replaced with a gas mixture of 77.7% helium and 22.3% argon. The second assumption is that no fission gases are released during the preconditioning phase of the PBF testing. If some fission gases were released from the fuel during fuel rod preparation or the preconditioning phase of the testing, lower fission gas release would occur during the high power operation.

An evaluation was made of the computer cost of modeling fission gas production and release. The performance of the test fuel rod during Saxton irradiation and PBF testing was calculated both using and bypassing the fission gas production and release model. For the calculations using the fission gas release model, the computer running time is 60 s. For the calculations bypassing the fission gas release model, the computer running time is 24 s.

5.2 Summary and Conclusions

The fission gas release model (FASTGRASS) has been examined by a comparison of the calculated and measured fission gas release in Rod 17 of the PBF test IE-3. On the basis of this comparison, the following conclusions result.

1. The FASTGRASS model is applicable to the calculation of fission gas release over a broad range of fuel temperatures. The applicable temperature range varies from room temperature to the fuel melting temperature.

2. During high power operation (>60 kW/m) the FASTGRASS model calculates 200% to 300% more fission gas release than measured.

3. The fission gas release model should only be used when necessary, i.e., when the amount of fission gas release is expected to be greater than 10% of the amount of fill gas. Use of the model should be restricted because the cost of a computer analysis is about a factor of three higher when using the fission gas release model than when bypassing the model.

6. ASSESSMENT OF CIRCUMFERENTIALLY VARYING COOLANT CONDITION MODELING

The capability of prescribing circumferentially varying coolant conditions is a feature of FRAP-T6 that is not in FRAP-T5. The capability is demonstrated by calculating the response of a fuel rod to a localized flow blockage. Depending upon the fuel rod power, film boiling is calculated to azimuthally propagate from the portion of the cladding bordering the region of reduced flow to the portion bordering normal flow.

The coolant conditions before the flow blockage are typical of the normal operation coolant conditions of a PWR. The flow blockage is assumed to occur at a time of 0.0 s. The flow in the coolant channel bounded by the azimuthal coordinates of 45 degrees and 135 degrees (see Figure 28) instantly decreases by a factor of two and then remains constant. The coolant conditions in the other channels are assumed not to change. The spatial distribution of the coolant conditions is shown in Figure 28.

The fuel rod is typical of a PWR fuel rod, except for a small gap size and a short length. The characteristics of the fuel rod are described in Table 19. The peak fuel rod power is assumed to be 50 kW/m (case 1) and 60 kW/m (case 2).

The calculated cladding surface temperature azimuthal variation for the 50 kW/m case is shown in Figure 29. At the start time of 0.0 s, steady state conditions exist and nucleate boiling occurs at all azimuthal positions on the cladding surface. The DNB ratio (critical heat flux/surface heat flux) at all positions is 1.36. Film boiling, as indicated by the increase in cladding surface temperature, begins less than 1 s after the localized flow reduction. Film boiling is confined to the portion of the cladding bordering the channel with reduced flow. The other portions of the cladding surface remain in the nucleate boiling mode of heat transfer.

The cladding surface temperature history for the 60 kW/m case is shown in Figure 30. At the start time, steady state nucleate boiling occurs on all portions of the cladding surface. The DNB ratio is 1.16. Film boiling begins less than 1 s after the localized flow reduction. For 2.5 s, film boiling is confined to the portion of the cladding surface

P_o = Initial Coolant Pressure = 15.17 MPa

G_o = Initial Mass Flux = 2712 Kg/m^2

H_o = Initial Enthalpy = 1.64 x 10^6 J/Kg

X_o = Initial Quality = 2.2%

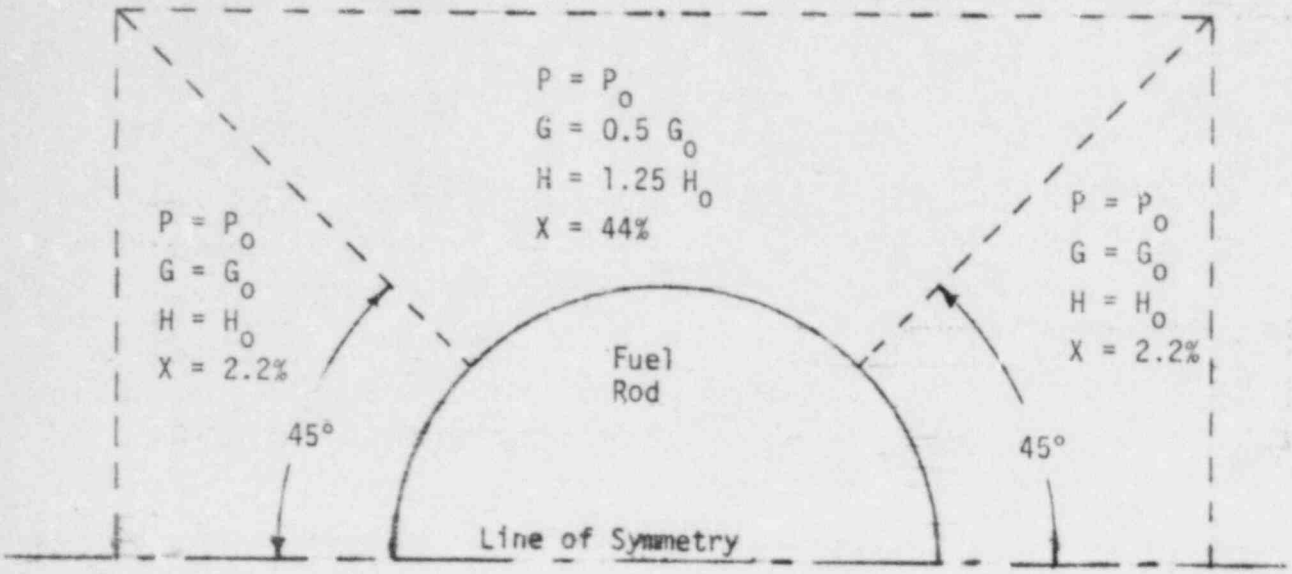

Figure 28. Spatial distribution of coolant conditions for a typical PWR rod.

TABLE 19. CHARACTERISTICS FOR FLOW BLOCKAGE ANALYSIS

Chacteristic	Value
Fuel Pellet Radius (mm)	4.267
Radial Fuel-Cladding Gap (mm)	0.071
Cladding Inside Radius (mm)	4.338
Cladding Outside Radius (mm)	4.925
Fuel Density (% Theoretical Density)	94.5
Fuel Stack Length (m)	0.904
Burnup (MW.s/kg)	0
Fill Gas	Helium
Fill Gas Pressure (MPa)	2.68

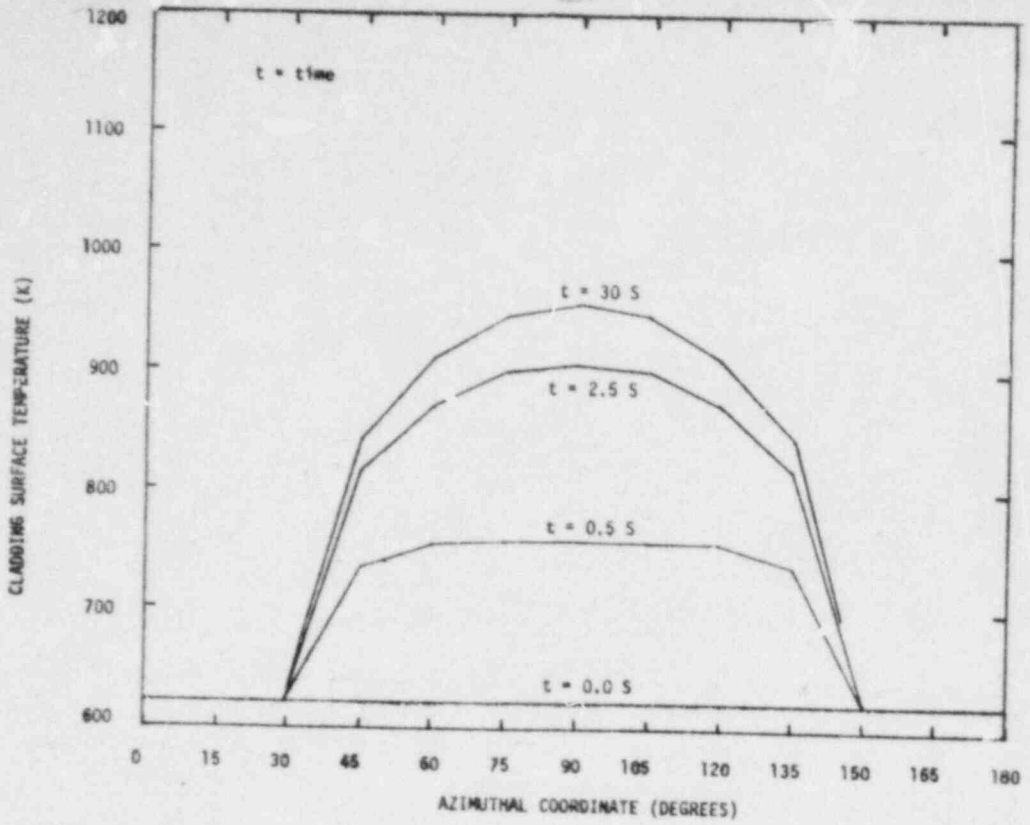

Figure 29. Azimuthal variation of cladding surface temperature for case 1 (50 kW/m).

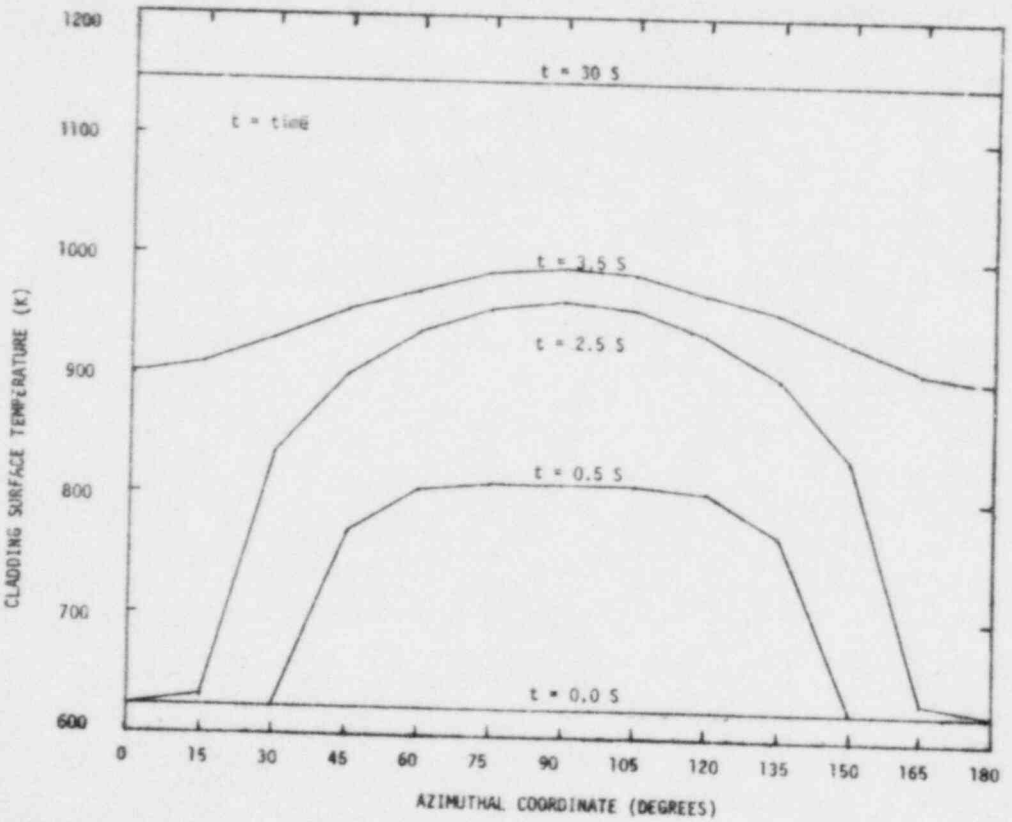

Figure 30. Azimuthal variation of cladding surface temperature for case 2 (60 kW/m).

bordering the channel with reduced flow. Then film boiling quickly propagates to all other circumferential locations. Steady state conditions again occur by the time of 30 s, and the entire cladding surface is near a temperature of 1140 K.

The surface heat flux history for the 60 kW/m case is shown in Figure 31. The cladding has a uniform heat flux prior to the flow reduction. After the localized flow reduction, the surface heat flux immediately decreases on the portion of the cladding bordering the channel with the flow reduction. The surface heat flux then increases in this region as the cladding surface temperature increases. The increasing cladding temperature causes a significant azimuthal temperature gradient in the cladding and a significant amount of heat flow toward the portion of the cladding still in nucleate boiling. The surface heat flux in the portion of the cladding in nucleate boiling increases and at a time of 2.5 s exceeds the critical heat flux at azimuthal positions of 30 degrees and 150 degrees, so that film boiling occurs. The film boiling quickly propagates in the azimuthal direction and occurs at all azimuthal positions.

7. ASSESSMENT OF ADDITIONAL FEATURES

The developmental assessment of FRAP-T6 tested the capabilities of several models in addition to those for which calculational results are presented in Sections 2 through 6. These models were exercised in one or more computer analyses, but the model calculations are not presented. The specific models and their cases of application are listed below.

1. The high temperature pellet-cladding mechanical interaction model is used in the computer analyses of PBF tests RIA 1-1 and RIA 1-2. For the RIA 1-1 test, the mechanical response calculations with FRAP-T5 would not continue beyond the time of the power burst. The mechanical response calculations

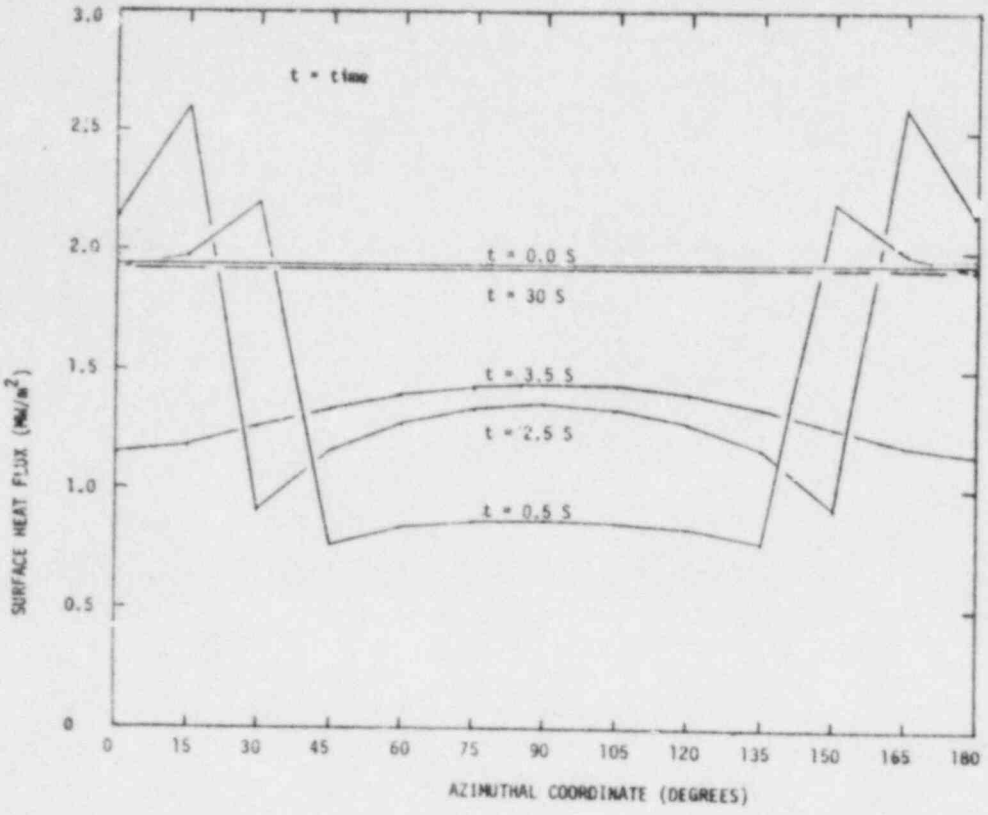

Figure 31. Azimuthal variation of cladding surface heat flux for case 2 (60 kW/m).

with FRAP-T6 are performed without difficulty from the beginning to the end of the transient.

2. The FRACAS-II model was used in a computer analysis of the HBWR IFA-508 test. The fuel rod thermal performance calculated with the FRACAS-II model is almost identical with that calculated using the FRACAS-I model with fuel relocation. However, the computer costs for the analysis with FRACAS-II is about a factor of three higher than the analysis with FRACAS-I. Use of the FRACAS-II model should be restricted to analyses focusing on the failure probability of the cladding during pellet-cladding mechanical interaction. Also, use of the FRACAS-II model is restricted to analysis of fuel rods with a cladding temperature less than 900 K because FRACAS-II does not model strain-rate effects which are dominant at cladding temperatures above 900 K.

3. The model for transient coolant enthalpy is used in the computer analysis of the TREAT FRF-2 test. The calculated cladding temperature is in good agreement with the measured cladding temperature. This good agreement indicates a correct calculation of the coolant enthalpy.

4. The cladding failure probability model in FRAP-T6 is used in all of the computer analyses performed for the developmental assessment of FRAP-T6. The calculations of the model are reasonable. Because the model is statistical in nature, a large number of computer analyses would be required for a quantitative assessment of the model. Therefore, the number of computer analyses performed for the developmental assessment are insufficient for a quantitative assessment.

5. The Chen correlation for nucleate boiling heat transfer is used in most of the computer analyses presented in this report. Prior to DNB, the calculated cladding temperature is in good agreement with the measured temperature. This good agreement indicates correct calculation of nucleate boiling heat transfer.

8. CONCLUSIONS

The developmental assessment of the FRAP-T6 code has achieved several objectives. The FRAP-T6 code has been checked for applicability and accuracy by comparing the code calculations with reliable experimental data. Reasons for discrepancies between the code calculations and the experimental data have been determined. The FRAP-T6 code calculations have been compared with calculations of its predecessor, FRAP-T5, to quantify modeling improvements. Also, the FRAP-T6 code has been exercised over a broad range of fuel rod transients to test the analysis capabilities for hypothetical reactor accidents.

Several conclusions have been drawn from the results of the FRAP-T6 developmental assessment.

1. The FRAP-T6 code is capable of analyzing fuel rod performance during operational transients and hypothetical reactor accidents. The capabilities of the code have been demonstrated by comparing code calculations with the results of several LOCA and RIA fuel rod tests. The proven capabilities of the code include the modeling of fuel stored energy, fuel rod cooling, cladding ballooning and high temperature pellet-cladding mechanical interaction.

2. The FRAP-T6 code can be expected to overpredict fuel rod temperatures by 0 to 5% prior to the time of DNB and by 0 to 20% after the time of DNB. The comparison of duplicate models has shown that the nonuniform gap model and the Groeneveld correlation for film boiling heat transfer give the best agreement with the experimental temperature data. For a large break LOCA, the code calculates DNB to occur 0 to 3 s earlier than observed. This discrepancy is the main reason for the overprediction of post-DNB fuel rod temperatures.

3. When using the FASTGRASS fission gas release model option, FRAP-T6 calculates transient fission gas release over a wide range of fuel temperatures. However, for high fuel rod powers, (>60 kW/m) the FASTGRASS model can be expected to overpredict

fission gas release by 200% to 300%. Because of the significant increase in computer cost (factor of 3) when using the FASTGRASS model, use of the model should be restricted to cases where the fission gas release is expected to be at least 10% of the initial fill gas.

4. Using the BALON2 cladding ballooning model, the FRAP-T6 code accurately calculates cladding ballooning including extent of ballooning and time of cladding rupture. The accurate calculation is attributed to modeling of local cladding thinning and including the effects of fuel rod heating and pressurization rates. An accurate calculation of the final ballooning strain is important when considering the extent of flow area blockage. FRAP-T5 can also provide an upper bound on the amount of cladding ballooning through use of the FRACAS-I model.

5. The FRAP-T6 code is improved over the FRAP-T5 because of improved modeling and increased modeling features. The improved modeling of the fuel-cladding gap conductance gives a more accurate calculation of fuel rod temperature and stored energy. The improvements in the mechanical response models give a more accurate calculation of cladding ballooning and high temperature pellet-cladding mechanical interaction. The cladding failure probability model is extended to take into account the effects of cladding fatigue, stress corrosion cracking and nonuniform cladding ballooning. Additional models in the FRAP-T6 code allow the modeling of circumferentially varying coolant conditions and transient coolant enthalpy rise. Finally the addition of a dynamic storage procedure and an improved initialization procedure give a computer running time that is 10 to 30% smaller than that of FRAP-T5.

6. The developmental assessment of FRAP-T6 has shown three areas in which improvements could be made to the code. First, for a large break LOCA, the calculation of post-DNB cladding temperatures could be significantly improved by a more accurate calculation of the time of DNB. Next, the calculation of fuel stored energy

using the relocation model for fuel deformation could be significantly improved by calculating the fuel-cladding gap conductance with the open gap model instead of the closed gap model. Finally, the calculation of cladding ballooning could be improved by a "stiffening" of the relation of stress to strain in the neighborhood of cladding yielding.

9. REFERENCES

1. L. J. Ybarrondo, Quarterly Technical Progress Report on Water Reactor Safety Programs Sponsored by the Nuclear Regulatory Commission's Division of Reactor Safety Research, January-March 1980, NUREG/CR-1400, EGG-2031, April 1980.

2. L. J. Siefken, et al, FRAP-T6: A Computer Code for the Transient Analysis of Oxide Fuel Rods, NUREG/CR-2148, EGG-2104, May 1981.

3. L. J. Siefken et al, FRAP-T5: A Computer Code for the Transient Analysis of Oxide Fuel Rods, NUREG/CR-0840, TREE-1281, June 1979.

4. J. R. Larson et al., PBF-LOCA Test Series Test LOC-11 Test Results Report, NUREG/CR-0618, TREE-1329, April 1979.

5. M. Uchida and M. Ichikawa, In-Pile Diameter Measurement of Light-water Reactor Test Fuel Rods for Assessment of Pellet-Cladding, Mechanical Interaction, Nuclear Technology 51, November 1980, pp. 33-44.

6. R. W. Miller and A. D. Appelhans, Measured Effects of Fuel Rod Internal Gas Pressure and Xenon Concentration in Operating Fuel Rods and a Comparison with Basic Theory and FRAP Calculations, EGG-TFBP-5222, August 1980.

7. D. T. Sparks et al., Power-Cooling-Mismatch Test Series Test PR-1, Quick Look Report, EGG-TFBP-5122, March 1980.

8. R. W. Garner et al., Gap Conductance Test Series-2 Test Results Report for Tests GC 2-1, GC 2-2, and GC 2-3, NUREG/CR-0300, TREE-1268, November 1978.

9. R. A. Lorenz and G. W. Parker, Final Report on the Second Fuel Rod Failure Transient Test of a Zircaloy-Clad Fuel Rod Cluster in TREAT, ORNL-4710, January 1972.

10. S. L. Seiffert et al., Reactivity Initiated Accident Test Series Test RIA 1-1 (Radial Average Fuel Enthalpy of 285 cal/g) Fuel Behavior Report, NUREG/CR-1465, EGG-2040, September 1980.

11. G. B. Peeler, et al., Power-Cooling-Mismatch Test Series, Test PCM-4, Test Results Report, TFBP-TR-190, June 1977.

12. T. R. Yackle et al, PBF-LOCA Test Series Test LOC-3 Quick Look Report, TFBP-TR-328, July 1979.

13. B. A. Cook et al., Reactivity Initiated Accident Test Series Test RIA 1-2 Fuel Behavior Report, NUREG/CR-1842, EGG-2073, January 1981.

14. L. C. Farrar et al., Irradiation Effects Test Series Test IE-3 Test Results Report, TREE-NUREG-1106, October 1977.

15. K. Vinjamuri, Fuel Swelling Due to Retained Fission Gas in Molten Fuel During High Temperature Transients, NUREG/CR-1236, EGG-2014, February 1980.

APPENDIX A

DIFFERENCES BETWEEN FRAP-T5 AND FRAP-T6

APPENDIX A

DIFFERENCES BETWEEN FRAP-T5 AND FRAP-T6

The FRAP-T5 code [A.1] is the predecessor of the FRAP-T6 code[A.2] and is the basis of FRAP-T6 development. FRAP-T6 is improved over FRAP-T5 in the areas of temperature modeling, mechanical response modeling and fission gas release modeling. The overall efficiency of FRAP-T6 is improved over FRAP-T5 by the addition of a dynamic storage procedure and streamlined programming. FRAP-T6 has a new input data processing package, which allows a clear identification of the data in the input deck and performs an expanded diagnosis of input errors.

In the area of temperature modeling, the differences between FRAP-T5 and FRAP-T6 are as follows.

1. The FRAP-T5 code uses the gap conductance model of the GAPCON-THERMAL-1 code[A.3] and the FRAP-T6 code uses a modification of the gap conductance model of the GAPCON-THERMAL-2 code.[A.4] The gap conductance model of the GAPCON-THERMAL-2 code is modified to account for a nonuniform fuel-cladding gap. The model is also modified to force continuity of the calculated gap conductance as the fuel-cladding gap closes and "hard" pellet-cladding mechanical interaction begins.

2. The FRAP-T5 code uses the Thom correlation for nucleate boiling heat transfer while the FRAP-T6 code uses the Chen correlation.

3. The FRAP-T5 code uses the modified Bromley correlation for pool film boiling heat transfer, while FRAP-T6 uses the combined modified Hsu and Bromley-Pomeranz correlation.

4. The Tong-Young and Condie-Bengston high flow film boiling correlations in FRAP-T6 are a modification of those in FRAP-T5.

5. The FRAP-T6 code includes the Hsu-Beckner correlation for critical heat flux. This correlation is not in FRAP-T5.

6. The FRAP-T6 code uses the generalized FLECHT correlation for calculating reflood heat transfer, which is applicable for flooding rates in the range of 10 to 254 mm/s. The version of the FLECHT correlation in FRAP-T5 is applicable for flooding rates in the range of 25 to 254 mm/s.

7. The FRAP-T6 code has a transient coolant enthalpy rise model. The coolant enthalpy rise model in FRAP-T5 assumes steady-state conditions.

8. The FRAP-T6 code models the thermal conductivity of partially melted fuel, while the FRAP-T6 code does not.

9. The cladding stored energy during the alpha to beta phase transition is more accurately calculated in FRAP-T6 than FRAP-T5.

In the area of mechanical response modeling, the differences between FRAP-T5 and FRAP-T6 are as follows.

1. The cladding ballooning model (BALON2) for FRAP-T6 calculates the cladding stress taking into account the local thinning of the cladding, while the model in FRAP-T5 (BALON1) does not. In addition, the effects of heating and pressurization rates are included in BALON2 but not in BALON1.

2. High temperature (>900 K) pellet-cladding mechanical interaction is modeled in FRAP-T6 but not in FRAP-T5.

3. The failure probability model of FRAP-T6 accounts for the effects of stress corrosion cracking, fatigue and nonuniform cladding ballooning. These effects are not taken into account with FRAP-T5.

4. The fuel relocation model in FRAP-T6 is applicable to preconditioned fuel rods, while the model in FRAP-T5 is applicable to fuel rods with no preconditioning.

5. In FRAP-T6, the FRACAS-I model with fuel relocation is similar to the FRACAS-II model neglecting stress induced deformation of the fuel. The similarities allow the code user to link FRAP-T6 calculations using FRACAS-I with FRAPCON-2[A.5] calculations using FRACAS-II. In FRAP-T5, the FRACAS-I and FRACAS-II

models are distinctly different.

The other differences between FRAP-T5 and FRAP-T6 are summarized as follows.

1. For initialization of burnup dependent variable, FRAP-T6 is linked with FRAPCON-2[A.5], while FRAP-T5 is linked with FRAPCON-1.[A.6]
2. The material property package in FRAP-T6 is MATPRO 11, Rev. 1,[A.7] while MATPRO-11 is in FRAP-T5.[A.8]
3. The FASTGRASS model[A.9] for fission gas release is in FRAP-T6, while the GRASS model[A.10] is in FRAP-T5.

REFERENCES

A.1 L. J. Siefken, M. P. Bohn, S. O. Peck and J. A. Dearien, FRAP-T5: A Computer Code for the Transient Analysis of Oxide Fuel Rods, NUREG/CR-0840,TREE-1281, June 1979.

A.2 L. J. Siefken, C. M. Allison, M. P. Bohn and S. O. Peck, FRAP-T6: A Computer Code for the Transient Analysis of Oxide Fuel Rods, NUREG/CR-2148, EGG-2104, May 1981.

A.3 C. R. Hann, C. E. Beyer, L. J. Parchen, GAPCON-THERMAL-1: A Computer Program for Calculating the Gap Conductance in Oxide Fuel Pins, BNWL-1778, September 1973.

A.4 C. E. Beyer et al., GAPCON-THERMAL-2: A Computer Program for Calculating the Thermal Behavior of an Oxide Fuel Rod, BNWL-1898, November 1975.

A.5 G. A. Berna et al., FRAPCON-2: A Computer Code for the Calculation of Steady State Thermal-Mechanical Behavior of Oxide Fuel Rods, NUREG/CR-1845, December 1980.

A.6 G. A. Berna and M. P. Bohn, FRAPCON-1: A Computer Code for the Steady State Analysis of Oxide Fuel Rods, NUREG/CR-1463, EGG-2039, May 1981.

A.7 D. L. Hagrman, G. A. Reymann and R. E. Mason, MATPRO-Version 11 (Revision 1): A Handbook of Materials Properties for Use in the Analysis of Light Water Reactor Fuel Rod Behavior, NUREG/CR-0497, TREE-1280, Rev. 1, February 1980.

A.8 G. A. Reymann et al, MATPRO - Version 11: A Handbook of Materials Properties for Use in the Analysis of Light Water Reactor Fuel Rod Behavior, NUREG/CR-0497 TREE-1280, February 1979.

A.9 Light-Water-Reactor Safety Research Program: Quarterly Progress Report, April-June 1980, NUREG/CR-1801, ANL-80-107, October 1980.

A.10 J. Rest, GRASS-SST: A Comprehensive Mechanistic Model for the Prediction of Fission Gas Behavior in UO_2 Based Fuels During Steady State and Transient Conditions, NUREG/CR-0202, ANL-78-53, June 1978.

APPENDIX B

COMPUTER ANALYSIS CASES

APPENDIX B

COMPUTER ANALYSIS CASES

The applicability and accuracy of the FRAP-T6 code are determined by comparisons of code calculations with the results of well characterized fuel rod tests. The capabilities of the code are tested by computer analyses of fuel rod performance during hypothetical reactor accidents. A total of 16 fuel rod tests and hypothetical accidents are analyzed with FRAP-T6. The computer analysis cases are listed below.

1. PBF LOC-11C test (Rod 3)[B.1]
2. HBWR IFA-508 test (Rod 13)[B.2]
3. HBWR IFA-430 test (Rod 2)[B.3]
4. PBF PR-1 test (Rods 1 and 4)[B.4]
5. PBF GC 2-1 test (Rods 501 and 503)[B.5]
6. PBF GC 2-2 test (Rod 522-3)[B.5]
7. TREAT FRF-2 test (Rod 12)[B.6]
8. PBF RIA 1-1 test (Rod 3)[B.7]
9. PBF PCM-4 test[B.8]
10. PBF LOC-3 test[B.9]
11. PBF RIA 1-2 test[B.10]
12. PBF IE-test (Rod 17)[B.11]
13. Hypothetical 200% Cold Leg Break in a PWR
14. Hypothetical Flow Blockage in a PWR

Microfiche copies of the printout of the computer analyses are available upon request. The printout gives a detailed description of each fuel rod test. For example, the axial power profile of each analyzed fuel rod is given. The microfiche copies are available from the Program Library at the Idaho National Engineering Laboratory.

REFERENCES

B.1 J. R. Larson et al., PBF-LOCA Test Series Test LOC-11 Test Results Report, NUREG/CR-0618, TREE-1329, April 1979.

B.2 M. Uchida and M. Ichikawa, In-Pile Diameter Measurement of Lightwater Reactor Test Fuel Rods for Assessment of Pellet-Cladding Mechanical Interaction, Nuclear Technology 51, November 1980, pp. 33-34.

B.3 R. W. Miller and A. D. Appelhans, Measured Effects of Fuel Rod Internal Gas Pressure and Xenon Concentration in Operating Fuel Rods and a Comparison with Basic Theory and FRAP Calculations, EGG-TFBP-5222, August 1980.

B.4 D. T. Sparks et al., Power-Cooling-Mismatch Test Series Test PR-1, Quick Look Report, EGG-TFBP-5122, March 1980.

B.5 R. W. Garner et al., Gap Conductance Test Series-2 Test Results Report for Tests GC 2-1, GC 2-2, and GC 2-3, NUREG/CR-0300, TREE-1268, November 1978.

B.6 R. A. Lorenz and G. W. Parker, Final Report on the Second Fuel Rod Failure Transient Test of a Zircaloy-Clad Fuel Rod Cluster in TREAT, ORNL-4710, January 1972.

B.7 S. L. Seiffert et al., Reactivity Initiated Accident Test Series RIA 1-1 (Radial Average Fuel Enthalpy of 285 cal/g) Fuel Behavior Report, NUREG/CR-1465, EGG-2040, September 1980.

B.8 G. B. Peeler, et al., Power-Cooling-Mismatch Test Series, Test PCM-4, Test Results Report, TFBP-TR-190, June 1977.

B.9 T. R. Yackle et al., PBF-LOCA Test Series Test LOC-3 Quick Look Report, TFBP-TR-328, July 1979.

B.10 B. A. Cook et al., Reactivity Initiated Accident Test Series Test RIA 1-2 Fuel Behavior Report, NUREG/CR-1842, EGG-2073, January 1981.

B.11 L. C. Farrar et al., Irradiation Effects Test Series Test IE-3 Test Results Report, TREE-NUREG-1106, October 1977.